Tampere University

Nekhel Das

SPONTANEOUS EMISSION ENHANCEMENT OF FLUOROPHORE BY PLASMONIC NANOANTENNA

ABSTRACT

Optical nanoantennas are very efficient for manipulating and controlling light. These nanoantennas support plasmonic oscillations and enhance the local field. This enhancement can be used in different applications. In this thesis, I have designed and fabricated metallic (plasmonic) nanodisks (NDs) array to enhance the emission of fluorescence dye molecules.

For emission enhancement, a fluorescence dye (LDS750) with an emission band (emission peak 650 nm) close to plasmon resonance of plasmonic nanoantenna is selected. Localized surface plasmon resonance of NDs depends on the size, shape as well as dielectric properties of the materials. The plasmonic nanodisks are designed to observe their interaction with LDS750 dye in the range of 600-700 nm wavelength. The proper geometry of the nanodisks is designed to achieve plasmon resonance, which spectrally overlaps with the emission spectrum of LDS750. Diameter and period of the nanodisk array have been varied to find out the best spectral overlap. The effect of these parameters on the optical response has been investigated numerically and experimentally. Simulations are performed using the Finite-Difference Time-Domain (FDTD) method.

The fabrication process of NDs is done by using electron beam lithography, electron beam evaporation process followed by development and lift-off. Investigated plasmonic NDs arrays are made of gold (Au) with periods of 360 nm, 400 nm and 440 nm while diameter range is in between 105-195 nm for each period. LDS750 fluorescence dye molecules are mixed with Ploymethyl methacrylate 2% solution in anisole (PMMA A2) as dielectric host medium. A layer of PMMA and LDS750 mix is added on top of the NDs to investigate the emission enhancement of LDS750.

The numerical and experimental study of the NDs and LDS750 hybrid system, provide how the parameters of the plasmonic nanodisks such as diameter, period and substrate, play significant roles in the enhancement of the emission of LDS750 dye. The time-resolved fluorescence spectroscopy results and Fluorescence Lifetime Imaging (FLIM) results are strong evidence of emission enhancement of LDS750 dye in the presence of NDs.

The interaction between the enhanced localize electric field of NDs and LDS750 modified the spontaneous emission by increasing the rate of LDS750 excitation. Consequently, the decay rate change of LDS750 due to the Purcell enhancement. The achieved results from this research would guide the design and fabricate plasmon hybrid system for practical applications.

Keywords: Nanoantenna, localized surface plasmon, emission enhancement, Purcell enhancement.

PREFACE

The research presented in this thesis has been conducted at Engineering and Natural Sciences Faculty of Tampere University (Hervanta Campus), Tampere, Finland. I have completed my dissertation under the supervision of Professor Humeyra Caglayan.

At first, I would like to express my heartiest gratitude to Professor Humeyra Caglayan for her support and encouragement throughout my thesis. Her provision, guidance and unconditional efforts helped me to improve my research work and competences substantially. The lab facilities in the Metaplasmonics group provided me wonderful research environment to obtain the results of this thesis.

I would like to thank Dr. Alireza Rahimi Rashed for his support during this research. Without his proper guidance and help, I would not be able to finalize my experiments and this thesis. He taught me the technical details as well as the physics of the experimental work. He approaches me like a big brother which makes the research fun and easier.

I am thankful to Dr. Bilge Can Yildiz for her continuous support during my thesis writing. Her assistance in writing helped me greatly to improve my thesis.

A heartful thanks to Mohsin Habib, without his effort and help during sample preparation, it was impossible to finish this thesis on time. His passion for his work not only makes my research convenient but also make me more enthusiastic.

I am grateful to be a member of such a wonderful group. I am thankful to all members of Metaplasmonics team for their excellent support during my thesis research.

My whole achievement belongs to my mother Nerupa Rani Das, who dedicated her life for my wellbeing and success with unconditional love. She has struggled her entire life to fulfil my dream after I lost my father in childhood. Her endless support and encouragement make me more enthusiastic and motivated.

Finally, I thank Almighty God, for the life and chance to achieve knowledge, wisdom.

Tampere, November 2019

Nekhel Das

CONTENTS

LIST OF FIGURES

LIST OF SYMBOLS AND ABBREVIATIONS

SERS	Surface-enhanced Raman spectroscopy
LSPs	Localized surface plasmons
LSPR	Localized surface plasmon resonance
SPPs	Surface plasmon polaritons
TM	Transverse magnetic
EM	Electromagnetic
PL	Photoluminescence
NIR	Near-infrared radiation
PMMA	Polymethyl methacrylate
QEs	Quantum emitters
QDs	Quantum dots
RET	Resonant energy transfer
NDs	Nanodisks
FDTD	Finite difference time domain
E-BEAM	Electron beam
EBL	Electron beam lithography
IPA	IsoPropylic Alcohol
Rpm	Revolutions per minute
EHT	Electron high tension
SEM	Scanning Electron Microscopy
CCD	Charged Coupled Device
AOTF	Acousto-optic tunable filter
Au	Aurum (Gold)
Al	Aluminum
FS	Fused silica
TSCPC	Time-Correlated Single-Photon counting
CFD	Constant function discriminator
TAC	Time to amplitude converter
APD	Avalanche photodiode
FLIM	Fluorescence-lifetime imaging microscopy
PMT	Photomultiplier tube
ALD	Atomic layer deposition
MHz	Megahertz
sec	Second
nm	nanometer
2D	Two-dimension
3D	Three dimension
D	Dielectric displacement
B	Magnetic induction
E	Electric field
H	Magnetic field
J_{ext}	External charge
ρ_{ext}	Current density
P	Polarization
M	Magnetization
ε_0	Vacuum electric permittivity
ε_m	Material electric permittivity
μ_0	Magnetic permeability
n	Refractive index
χ_e	Dielectric susceptibility
e	Electron charge
m_e	Electron mass

ω	Angular frequency
β	Propagation constant
k_0	Wave vector in vacuum
ε_d	The permittivity of a dielectric medium
C_{abs}	Absorption cross-section
C_{sca}	Scattering cross-section
C_{ext}	Extinction cross-section
α	Polarizability
$\Re[\varepsilon_m]$	The real part of permittivity in materials
$\Im$	Imaginary part
I_{sca}	Scattered intensity
L_i	Geometrical form factor
V	Volume
ω_{LSPR}	Resonance frequency
ω_p	Plasma frequency
S_0	Singlet ground state
T	Triplet state
E	Energy
h	Planck's constant
ν	Photon frequency
γ_r	Radiative decay rate
γ_{nr}	Non-radiative decay rate
T	Time
τ	Fluorescence lifetime
ϕ	Quantum yield
k_T	Energy transfer rate
r	Distance between donor-acceptor
χ	Coupling constant
d	Dipole moment
$P_{0,rad}$	Radiative power
c	Velocity of light
F	Purcell factor
γ_{Em}	Emission enchantment factor
C	Celsius

1. INTRODUCTION

Plasmonic nanostructures have opened a new door for many applications which require nanoscale control on the light-matter interactions such as biosensing [1] and enhanced light emission [2,3]. A plasmonic nanoantenna can confine light beyond the diffraction limit and enhance the local field. Due to these properties; fluorescence enhancement, multiphoton absorption and SERS (Surface-enhanced Raman spectroscopy) have been observed by many researchers [4–8].

In most of these studies, a metallic nanoparticle used as a plasmonic nanoantenna. The properties of a metal nanoparticle govern by the size, shape and dielectric environment [9–12]. It has been shown that the absorption band of a Gold (Au) nanoparticle shifts to longer wavelengths as the diameter increases [9]. The scattering and extinction cross-section of nanoparticles depends on the polarizability, and polarizability depends on the shape of the nanoparticle as well as the surrounding medium's dielectric constant. Solvent surrounding the nanoparticles, and/or the substrate that nanoparticles placed modify the plasmon resonance wavelength.

Tunability of the electromagnetic properties is obtained by changing the size of the nanoantenna. Size modification of the nanoantenna changes the localized surface plasmon resonance (LSPR) [13,14]. LSPR can also be tuned by changing the shape of the nanoantenna. Different shape of nanoantenna has been studied. The shape like dots, bowties and rods enhance the possibility of plasmon resonance tuning. If nanoantenna is rod-shaped there will be two plasmon oscillations, one along short and one along the long axis. Modification of any of the axis will change LSPR with respect to that axis [15–18]. Bowtie nanoantenna is another shape which also has the possibility to tune the plasmon resonance [19]. Spectral response of bowtie nanoantenna can be changed by changing the length and width of it [20–25]. Polarization of incident light plays an important role in plasmon resonance in the shape of nano-rod and bowtie nanoantennas. Although it is not as effective as the other parameters, by changing the polarization angle, it is possible to change the spectral position of plasmon resonance [26–32].

Fluorescence of an emitter can occur via radiative or non-radiative decay channels. Engineering the radiative decay of emitters with plasmonic nanostructures is one of the scientific challenges in this field. Emission enhancement of fluorescence materials with

plasmonic nanoantennas studied by separate groups [33,34]. Recent studies show promising results on the radiative decay rate modification of the emitters embedded in nanoantennas or in the close vicinity of plasmonic antennas. The hybrid system of a metal nanoparticle and fluorophore can enhance local excitation field as well as change radiative and non-radiative decay rate of the fluorophore. This is observed also as a change in the lifetime and quantum yield when absorption band of the gold nanoparticle and emission band of the fluorescence species overlap [35]. 3 to 1.5-fold fluorescence enhancement is presented by changing the diameter of gold nanoparticle and spectral overlap variation. The distance between nanoparticle and emitters also play a vital role in the emission enhancement [35]. In another study, it has been shown that single nano-particle can enhance the radiative decay rate of emitters (Atto 680) around 5-folds [4,36]. They have shown the enhancement alteration in the rate of emission and excitation by precise variation of the antenna parameter and plasmonic mode spectrum.

Moreover, the enhancement factor depends on the shape of the nanoparticle. Gold (Au) nanosphere can enhance either excitation or emission because it supports one plasmon mode. On the other hand, Au nanorods further enhance the excitation and emission of the emitters with dual plasmon modes (transversal and longitudinal surface plasmon res-onance). The shorter axis of the nanorods produce transversal resonance, which en-hances the excitation and longer axis create longitudinal resonance for enhancing the emission of emitters [37].

The effect of substrate or environment in plasmon resonance is numerically and experi-mentally investigated. If the structure is surrounded by a solvent, the plasmon resonance is modified because the plasmon wavelength depends on the dielectric constant of the medium and dielectric constant change based on the solvent refractive index [15,38–45]. Furthermore, when the structure is in a dielectric medium there is higher energy confine-ment (lower resonance wavelength) [46,47]. In the presence of the dielectric medium, the local electric field is changed, which can enhance the emission of fluorescence mol-ecules placed in the vicinity of the nanoantenna [4,48,49]. On the other hand, the plas-mon resonance peak becomes broader with the increase of the refractive index of the surrounding medium.

The scattering and absorption band wavelength can change in different dielectric envi-ronment (substrate and solvent), which are investigated by different research groups [50–52]. They have presented that Ag (silver) nanoparticle has higher extinction on the glass then mica. Consequently, the external environment (substrate) has an effect on the localized surface plasmon resonance (LSPR). LSPR is red-shifted with the increase of the refractive index of the substrate [53,54]. Ag nanoparticle area of contact with the

substrate has changed the LSPR toward redshift when it sinks in the substrate [51]. Accordingly, nanoantenna position on substrate and dye layer placement is important. Because it will change the plasmon resonance of nanoantenna and emission enhancement factor of fluorescence materials. If the dye layer is at the bottom of the nanoantenna it will decrease the substrate effect. When the dye layer is on top of nanoantenna, it will affect both plasmon resonance of nanoantenna and the dye molecules emission spectrum modification.

In this thesis, the effect of the shape, size, and substrate to the plasmon resonance band of nanoantenna array is investigated to enhance the emission of emitters. We have designed circular shape Au nanodisks (NDs) as plasmonic nanoantenna. Nanodisk is a polarization independent structure and can be fabricated with standard nanofabrication techniques. Resonance band of the NDs is easy to optimize by changing its diameter and period of the array. The NDs array with a different period, size and substrate are fabricated and measured. In this project, we investigated the emission enhancement of the emitters in the presence of the plasmonic nanodisk arrays. The presence of plasmonic nanodisks modifies the emitters emission and lifetime. Tailoring the plasmon resonance band provides the spectral overlap of the emitter emission spectrum for efficient energy transfer. Furthermore, we observed the excitation power dependence of the emission intensity, as well as the influence of the distance between the nanoantenna and emitters in the energy transfer.

This thesis starts with an overview of the theory of plasmons. In the following parts, general information on the energy transfer process, enhancement of the dye molecules emission is described. Finally, the optimized shape of the nanodisk, substrate selection and proper hybrid system for the energy transfer process with emission enhancement of fluorophore are described and supported with experimental data.

2. THEORY OF PLASMONIC NANOANTENNAS AND PHOTOLUMINESCENCE PROCESS

Free electrons can be resonantly excited when they interact with light in a range of optical frequencies. In the span of these frequencies, free electrons of metal can sustain collective oscillations in the charge density, known as *plasmons,* with distinct resonance. Existence of plasmons is a characteristic of the interaction between light and metal. Surface plasmons, associated with the surface charge density, can produce strongly enhanced optical near-fields confined on the metal-dielectric interface [55]. Plasmonics is the study of the relation of this optical phenomenon and the electromagnetic response of metals [55]. In this chapter, first of all, the theoretical concept of plasmonic and plasmonic nanoantennas is described. Then, fluorescence property of the emitters and decay rate modification of the emitters due to these nanoantennas are elaborately discussed.

2.1 Plasmonics

The plasmons, which are the collective oscillations of free electrons, emerge due to the interaction with the external electric field. This follows from the solution of Maxwell's equations subject to particular boundary conditions. Macroscopic Maxwell's equations are the following,

$$\nabla . \boldsymbol{D} = \rho_{ext}, \tag{2.1.1}$$

$$\nabla . \boldsymbol{B} = 0, \tag{2.1.2}$$

$$\nabla \times \boldsymbol{E} = -\frac{\partial \boldsymbol{B}}{\partial t}, \tag{2.1.3}$$

$$\nabla \times \boldsymbol{H} = \boldsymbol{J}_{ext} + \frac{\partial \boldsymbol{D}}{\partial t}, \tag{2.1.4}$$

where, $\boldsymbol{D}, \boldsymbol{E}, \boldsymbol{H}$ and $\boldsymbol{B}$ are the dielectric displacement, the electric field, the magnetic field, and the magnetic induction, respectively. Here, $\boldsymbol{J}_{ext}$ and ρ_{ext} are the external charges and current densities [56]. These equations link up with two other terms, polarization, $\boldsymbol{P}$ and magnetization, $\boldsymbol{M}$ by,

$$\boldsymbol{D} = \varepsilon_0 \boldsymbol{E} + \boldsymbol{P}, \tag{2.1.5}$$

$$\boldsymbol{H} = \frac{1}{\mu_0} \boldsymbol{B} - \boldsymbol{M}, \tag{2.1.6}$$

where ε_0 and μ_0 are the vacuum electric permittivity and magnetic permeability. In most cases, we are interested in the optical response of the metals in the frequency domain

[57]. Therefore, by taking the Fourier transform of time and space-dependent displacement, we can derive the frequency-dependent displacement as follows,

$$D(\omega) = \varepsilon_0 \varepsilon_m(\omega) E(\omega), \tag{2.1.7}$$

where $\varepsilon_m(\omega)$ is the dielectric function of the material, in which the electromagnetic wave propagates. In the case of the nonmagnetic medium, the magnetic response M vanishes. The material responses to the incident electric field by dipolar charge alignments, which creates dipole moments. Polarization, P is described by the electric dipole moment of the material per unit volume; it is related to the internal charge density ($\nabla \cdot P = -\rho$). For linear media, polarization is defined as follows,

$$P(\omega) = \varepsilon_0 \chi_e(\omega) E(\omega), \tag{2.1.8}$$

where $\chi_e(\omega)$ is called the dielectric susceptibility. From equations 2.1.5 to 2.1.8 we can write,

$$D(\omega) = \varepsilon_0 \varepsilon_m(\omega) E(\omega) = \varepsilon_0 E(\omega) + P(\omega). \tag{2.1.9}$$

Simplifying this equation, we get the expression for the dielectric function in terms of the dielectric susceptibility,

$$\varepsilon_m(\omega) = 1 + \chi_e(\omega). \tag{2.1.10}$$

This equation is the frequency-dependent dielectric function of materials [55]. To describe the optical properties of metals, we can use the plasma model where the free electron gas moves against the fixed positive ions. This displacement creates a positive charge in the lattice forming a restoring force.

The incident field, $E(r,t) = E_0(r)e^{-i\omega t}$ displaces the electrons with force, $F(r,t) = e\,E(r,t)$. Then, the equation of motion for an electron in plasma is expressed as,

$$m_e \frac{\partial^2 r}{\partial t^2} + m_e \gamma \frac{\partial r}{\partial t} = e E_0 e^{-i\omega t}, \tag{2.1.11}$$

which is known as the Drude- Summerfield model [55,57]. Here γ is the frequency of the collisions between electrons, which corresponds to the damping, e is the electron charge, and m_e is the mass of the electron. In the right-hand side of the equation 2.1.11, $E_0 e^{-i\omega t}$ is the incident field, which drives the electrons, generating oscillations in the form of $r(t) = re^{-i\omega t}$. Inserting this into the equation 2.1.11, we have:

$$r(\omega) = \frac{\frac{e}{m_e}}{\omega^2 + i\gamma\omega} E(\omega). \tag{2.1.12}$$

Microscopic polarization for the displaced electron is defined as $P = -ner$; therefore, we have,

$$P = -\frac{ne^2}{m(\omega^2 + i\gamma\omega)}E(\omega),$$

(2.1.13)

From the equations 2.1.5 and 2.1.13, the displacement, D is expressed as follows,

$$D = \varepsilon_0\left(1 - \frac{\omega_p^2}{\omega^2 + i\gamma\omega}\right)E(\omega).$$

(2.1.14)

Combining the equations 2.1.7 and 2.1.14, we have

$$\varepsilon_m(\omega) = 1 - \frac{\omega_p^2}{\omega^2 + i\gamma\omega}.$$

(2.1.15)

Here $\omega_p = \sqrt{\frac{ne^2}{\varepsilon_0 m_e}}$ is the plasma frequency.

This can be divided into real and imaginary parts as follows,

$$\varepsilon_m(\omega) = 1 - \frac{\omega_p^2}{\omega^2 + \gamma^2} + i\frac{\gamma\omega_p^2}{\omega(\omega^2 + \gamma^2)}.$$

(2.1.16)

Materials are characterized by the imaginary and real parts of their dielectric function (dispersion). For instance, a negative real part of the dielectric function means that the light cannot penetrate through the material (i.e. not more than the skin depth) [57], as in the case of metals. The imaginary part describes the dissipation of energy associated with the motion of electrons.

A good plasmonic material, such as gold and silver, is identified via the real and imaginary parts of its dielectric function. If the following property is satisfied, the material is referred as a good plasmonic material [58],

$$\Re[\varepsilon_m(\omega)] < 0, \ \Im[\varepsilon_m(\omega)] \ll -\Re[\varepsilon_m(\omega)].$$

(2.1.17)

The metals with the properties given in 2.1.17, can support plasmon oscillations, which are classified into two different types. One of them, localized surface plasmons (LSPs), which is the interest of this study, are supported by plasmonic particles in nano-dimensions. The second type is the propagating counterpart of the LSPs, which is called surface plasmon polaritons (SPPs), supported by metal-dielectric interfaces.

2.1.1 Surface plasmon polaritons

Surface plasmon polaritons (SPPs) are electromagnetic waves, which propagate on the metal-dielectric interfaces. The dispersion of the supported SPPs can be obtained by solving Maxwell's equations with appropriate boundary conditions [59].
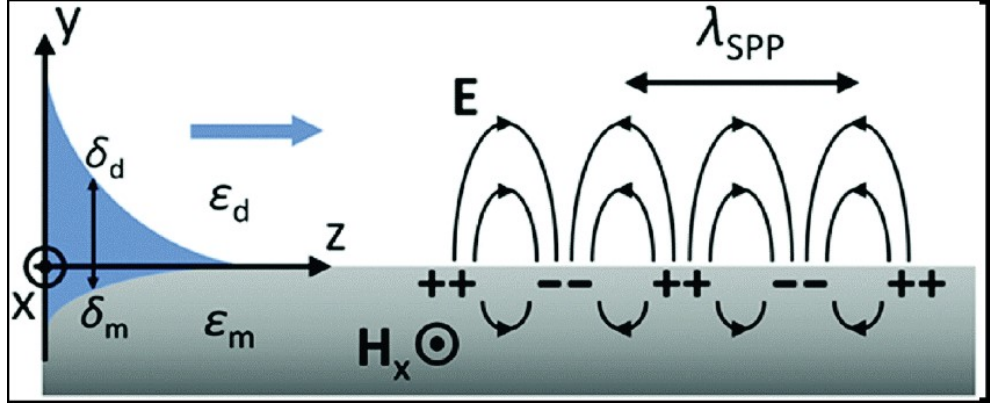
Figure 1. *SPP propagation in the interface of a metal and dielectric, adopted from Ref. [60].*

Here, we consider a transverse magnetic (TM) wave propagating on the metal-dielectric interface. A TM wave refers to an electromagnetic wave where its electric field component is perpendicular to the interface, as shown in Figure 1. The wave equation for the TM wave is given as,

$$\frac{\partial^2 H_y}{\partial z^2} + (k_0^2 \varepsilon - \beta^2)H_y = 0, \tag{2.2.1}$$

where, H_y is a magnetic field component in the y-axis, β is the propagation constant in of the propagation direction (in Figure 1, z-direction), k_0 is the wave vector of the propagating wave in vacuum, ε is the dielectric constant of the medium. Boundary conditions dictate the following equation, which relates the propagation constants, $k_{m,d}$ and permittivity, $\varepsilon_{m,d}$ of metal (m) and dielectric (d) medium.

$$\frac{k_d}{k_m} = -\frac{\varepsilon_d}{\varepsilon_m}, \tag{2.2.2}$$

By putting the value of $H_y = A_n e^{i\beta x} e^{k_n z}$ (here n = m or d) in equation 2.2.1 for each medium, we have

$$k_m^2 = \beta^2 - k_0^2 \varepsilon_m, \tag{2.2.3}$$

$$k_d^2 = \beta^2 - k_0^2 \varepsilon_d. \tag{2.2.4}$$

Combining the equations 2.2.2, 2.2.3 and 2.2.4, we obtain the dispersion relation of SPPs as follows,

$$\beta = k_0 \sqrt{\frac{\varepsilon_d \varepsilon_m}{\varepsilon_d + \varepsilon_m}}.$$

(2.2.5)

Equation 2.2.5 is the dispersion relation of SPP waves on a metal-dielectric interface. As shown in Figure 1 SPP dispersion curve always lies beyond the light line (incident electromagnetic propagation), which means SPP modes cannot be excited directly on flat interfaces. There are ways to excite SPP modes, such as grating coupling, and Kretschmann geometry, where the geometrical and/or optical features provide the required momentum.

2.1.2 Localized surface plasmons

Localized surface plasmons (LSPs) are the non-propagating collective charge oscillations supported by metal nanostructures [57,59,61]. When light is illuminated on a plasmonic nanostructure, it drives the free electron oscillations, against the restoring force due to the Coulomb interaction, enabling a resonance. This is called localized surface plasmon resonance (LSPR). LSP field is a very strong localized field around the nanoparticle (three orders of magnitude than excitation for nanowire in reference [62]), which decays very fast away from the nanoparticle. Localized field intensity depends on the size of nanoparticles and the surrounding medium. Bulk or massive particles cannot support LSPs. In other words, to obtain LSP oscillations, the diameter of the particle needs to be much smaller than the wavelength of the incident light [57]. Incident field induces a charge distribution on the surface of the nanoparticle, which is usually characterized as an electric dipole.

Coupling of free electrons on a nanostructure with the incident photons depends on the size and shape of the nanostructure as well as the dielectric function of the medium and material of the nanostructure [63]. This coupling efficiency can be described via the absorption (C_{abs}) and scattering (C_{sca}) cross-sections of the nanostructure. These cross-sections can be much larger than the geometrical cross-section of the nanostructure. Therefore, they quantify the strength of the electric field inside and outside of the structure [58].
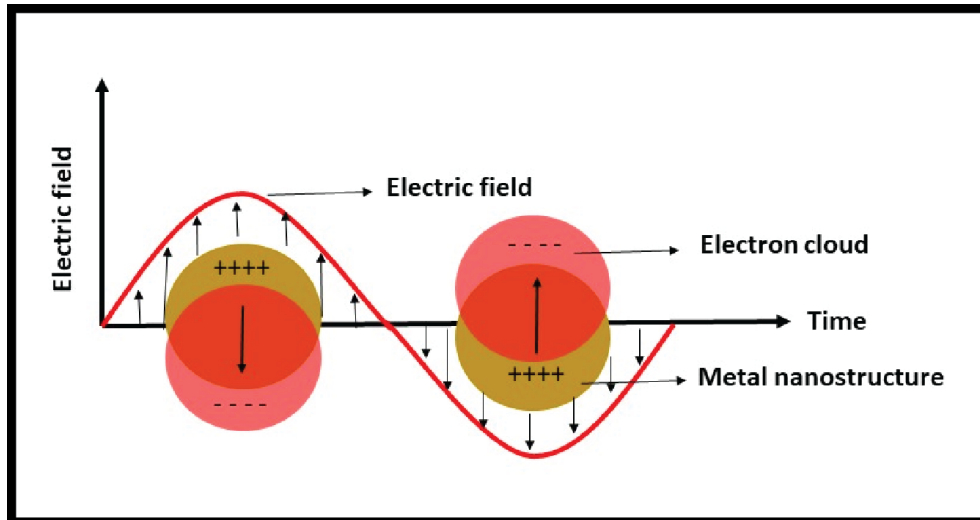
Figure 2. *Surface plasmon resonance of a nanostructure due to the interaction between the conduction electrons and the electromagnetic field* [64] *.*

The material, shape and size of the nanoparticles determine the LSPR. For simplicity, we consider the example of a nanosphere in this section of the thesis. Figure 2 portrays the LSP oscillations on a nanosphere as a function of time. Induced charge density generates the LSP field. The charge separation induces a dipole moment, and the strength of the dipole moment depends on the polarizability α [65]. The polarizability of a nanosphere is expressed by the Clausius-Mossotti relation, as follows,

$$\alpha(\omega) = 4\pi R^3 \frac{\varepsilon_m - \varepsilon_d}{\varepsilon_m + 2\varepsilon_d}. \tag{2.3.1}$$

Where, R is the radius of the sphere, ε_m and ε_d are the dielectric functions of the metal and the surrounding dielectric medium, respectively. If we assume that the dielectric function of a dielectric medium ε_d is constant, then it is possible to find the maximum polarizability for a frequency. The maximum polarizability α occurs at the frequency when $\varepsilon_m + 2\varepsilon_d$ is minimum and the condition $\Re[\varepsilon_m] + 2\varepsilon_d = 0$ is satisfied.

The following section will discuss more the polarizability of a nanoantenna to define the LSPR.

2.1.3 Light scattering properties of plasmonic nanoantennas

Localization of the electromagnetic (EM) energy in subwavelength dimensions (i.e. hot spots) due to the plasmons are interesting for many applications. For example, EM energy transfer from near to far-field (or vice versa), becomes more efficient in the LSPR frequency. This property makes plasmonic nanostructures act as nanoantennas that work similarly to the radio antennas at higher frequencies.

Optical nanoantennas are used to modify and regulate the radiation in the optical regime [66]. Interaction of light with a metal nanostructure is dependent on the shape, size and dielectric function of the metal, as well as the surrounding medium. Scattering and absorption, which quantify the interaction of the nanoantenna with the incident light, are the fundamental characteristics of localized plasmon resonance. An oscillating dipole is generated on the nanoparticle by the incident light. This oscillating dipole radiates electromagnetic field, which is called scattering. Scattering cross-section of the nanostructure is expressed as [57,67],

$$C_{sca} = \frac{k^4}{6\pi}|\alpha|^2 = \frac{8\pi}{3}k^4 a^6 \left|\frac{\varepsilon_m - \varepsilon_d}{\varepsilon_m + 2\varepsilon_d}\right|^2. \tag{2.4.1}$$

Here k is the wave vector, α is the polarizability, ε_m and ε_d are the dielectric functions of the metal and the dielectric constant of the surrounding medium, respectively. Similarly, absorption cross-section is expressed as [56],

$$C_{abs} = k\Im[\alpha] = 4\pi k\alpha^3 \Im\left[\frac{\varepsilon_m - \varepsilon_d}{\varepsilon_m + 2\varepsilon_d}\right]. \tag{2.4.2}$$

Scattered intensity depends on the scattering cross-section by $I_{sca} = \frac{I_0(\omega)C_{sca}}{A}$. Here A is the geometrical cross-section of nanoantenna and $I_0(\omega)$ is the intensity of the incident light. Extinction cross-section is defined by the sum of the scattering and absorption cross-sections, i.e. $C_{ext} = C_{abs} + C_{sca}$. [57] Strong interaction with light provides absorption and scattering cross-section exceeding the geometrical cross-section of the nanoantenna [68].

$$C_{ext} = 9\frac{\omega}{c}\varepsilon_m^{\frac{3}{2}}V \frac{\varepsilon_2}{[\varepsilon_1 + 2\varepsilon_d]^2 + \varepsilon_2^2} \tag{2.4.3}$$

Here ε_1 and ε_2 are the real and imaginary parts of the dielectric function of the metal. Extinction cross-section indicates the amount of the EM field removed from incoming light by the nano-structure.

Scattering and absorption properties given above are for a nanosphere. In this study, we investigate nanodisks. Therefore, polarizability, scattering and absorption cross-section expressions are modified for our case. For ellipsoid orientation along the axis (x, y, z) the factor used is known as geometrical form factor. Size of the ellipsoid in (x, y) plane and the size in z plane denote the specific shape of the ellipsoid as a sphere (x =y=z), prolate spheroid x=y and x, y < z. However, nanodisks could be considered as oblate spheroids (a=b>c) with axis x=a, y=b and z=c. Here, a=b=diameter and c= height of the nanodisk. The geometrical form factor L_i helps to adjust the polarizability of the sphere to disk. By solving Laplace's equation for L_i

$$L_i = \frac{abc}{2} \int_0^\infty \frac{ds}{(s + r_i^2)\sqrt{(s + a^2)(s + b^2)(s + c^2)}}. \tag{2.4.4}$$

Here $i \in \{x, y, z\}$ now for the oblate spheroids L_z can be analytically expressed as

$$L_z = \frac{1}{e^2 \left(1 - \frac{\sqrt{1 - e^2}}{e} \arcsin e\right)}. \tag{2.4.5}$$

Where, $e = \sqrt{\frac{a^2 - c^2}{a^2}}$.

The geometrical form factor depends on the ratio of the vertical and horizontal semi-axis of the spheroid. In the case of nanodisks, its diameter and height ratio are not the same as nanosphere. Then, equation 2.3.1, which is the polarizability of a nanosphere, is modified for an oblate spheroid along an arbitrary axis (x, y, z), as follows,

$$\alpha_i = V \frac{\varepsilon_m - \varepsilon_d}{\varepsilon_d + L_i(\varepsilon_m - \varepsilon_d)}. \tag{2.4.6}$$

where, $V = \frac{4}{3}\pi abc$ is the volume of the oblate spheroid. Eq. 2.4.6 confirms that polarizability of an oblate sphere (or approximately a nanodisk) depends on the size, geometrical form factor of the nanostructure, and the dielectric properties of the nanostructure and the surrounding medium [10,69]. One can obtain scattering and absorption cross-sections of a nanodisk by employing equation 2.4.6 to equations 2.4.1, 2.4.2 and 2.4.3, instead of the polarizability for nanospheres. By inserting the value of ε_m from equation 2.1.15 in equation 2.4.6 and by simplification, we can derive the equation of resonance frequency,

$$\omega_{LSPR} = \frac{\omega_p}{\sqrt{1 + \left(\frac{\alpha}{\alpha L_i - V} - 1\right)\varepsilon_d}} \tag{2.4.7}$$

This is a resonance frequency mentioned in section 2.1.3 for maximum polarizability. Note that the damping factor is neglected in equation 2.4.7.

At the scattering resonance, due to the high field intensity, the interaction of plasmons with quantum emitters can generate emission enhancement. Photoluminescence of the quantum emitters also depends on the excitation of the emitters because a sufficient amount of energy is needed for exciting the ground-state electron to excited state. In the next section, the photoluminescence process for quantum emitters and the enhancement of this process by the nanostructure will be briefly discussed.

2.2 Photoluminescence

Photoluminescence (PL) is the process where chromophore (i.e. fluorescence dye, quantum dots) emits photons after absorbing the incident photon from a light source [70]. This phenomenon is classified as fluorescence and phosphorescence. Photoluminescence happens when an excited electron loses its energy and go through vibrational relaxation channels to return the ground state. However, relaxation can occur by non-radiative decay which produces heat by vibrations or collisions [71].
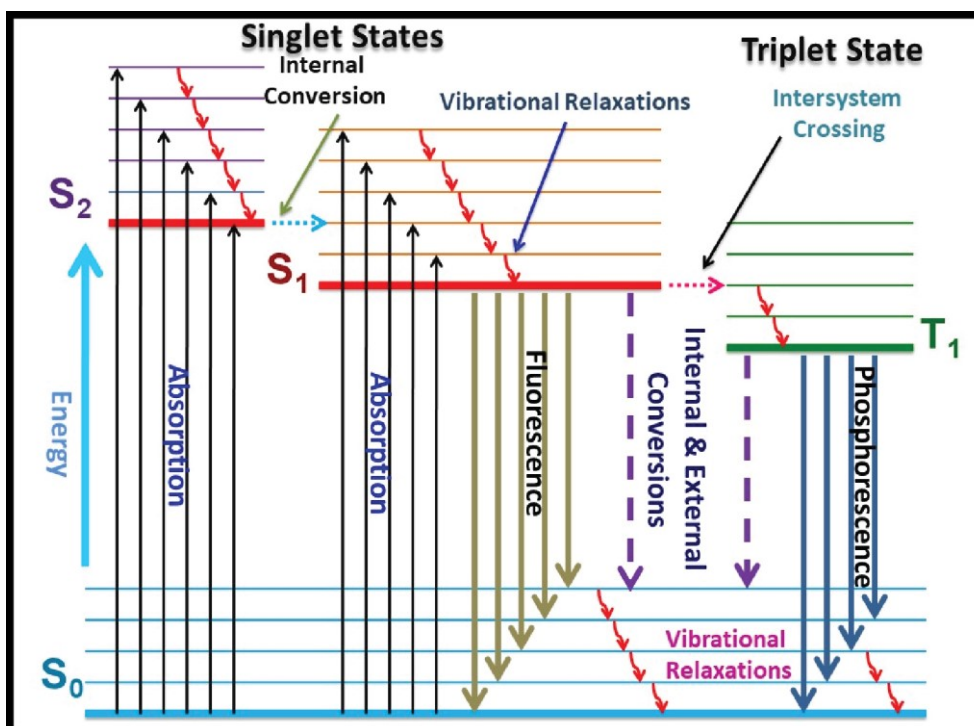
Figure 3. *Jablonski diagram illustrating the fluorescence and phosphorescence process* [72].

Jablonski diagram, shown in Figure 3, illustrates the energy levels, excitation and relaxation processes of a fluorescent molecule via radiative and non-radiative channels [73]. Excited and ground states have different energy levels, which are defined by $E = h\nu$, where h is the Planck's constant and ν is the frequency of the photon. For fluorescence, minimum energy to excite an electron from a ground state with energy E_0, to an excited state, with energy, E_1 is ΔE, where,

$$\Delta E = E_1 - E_0 = h\nu_1 - h\nu_2. \tag{2.5.1}$$

This amount of energy can be obtained by light. As a result, a molecule absorbs light, and its electrons are transferred from the ground states to an excited state. First, the electron undergoes vibrational relaxations within the same electronic state, to the lowest level of a singlet state by internal conversion and vibrational relaxations. Internal conversion is a non-radiative process, which is shown in Figure 3 as the blue dashed arrow,

and it occurs between two same spin states. The upward vertical arrows represent the absorption of light (electromagnetic energy) at specific wavelengths which excites the electron from the ground state to excited state ($S_0 \rightarrow S_1, S_2$). The red downward arrows indicate the vibrational relaxation between vibrational energy levels of electronic states. Green and blue vertical downward arrows from $S_1 \rightarrow S_0$ and $T_1 \rightarrow S_0$ show the emission of electromagnetic energy. These two transitions are known as fluorescence and phosphorescence, respectively.

When photoluminescence occurs from singlet state to ground state, it is called fluorescence, and it has a very short lifetime. The fluorescence process, time for absoption and emission is very short. Time duration for absorbed energy to promote electron from ground state to excited state is approximatly 10^{-8}s while to return the ground state time taken by the elctron in order of 10^{-15} s [73]. The photon emission from triplet state to ground state is known as phosphorescence. This process is a slow process compared to fluorescence. Phosphorescence does not emit immediately because it goes through an energy state transition between singlet and triplet. From the Jablonski diagram, it is seen that the fluorescence energy is lower than the absorption energy. The energy difference between the absorption and emission is referred to as the Stokes shift [72–74]. Figure 4 shows the absorption and emission spectra of a fluorescence material [74]. It is seen that the material emits at longer wavelengths than the wavelengths at which it absorbs light. The shift in the spectra means that it loses energy during the emission process.
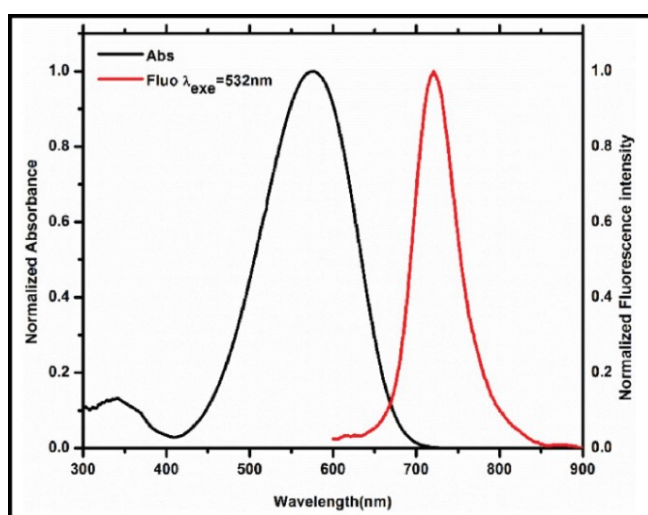
Figure 4. *Stokes shift between absorbance (black line) and emission spectra (red line)* [74].

Another energy loss mechanism is the *intersystem conversion*, which refers to non-radiative transition among different spin states. In Figure 3, the pink dashed arrow from singlet to triplet states indicates the intersystem crossing or conversion [75]. Electrons in S_1

can also exhibit spin conversion between triplet states, T_1. Populating the triplet states is not possible by direct absorption. It can occur only due to the transition from the lowest singlet to triplet states. Energy and spin of the electron, which undergoes *intersystem crossing*, are relaxed into a triplet state. The average lifetime of this transition is $10^{-3}\ s$ [76]. This process depends on the type of fluorescence materials and their properties.

2.2.1 Fluorescent materials

Fluorescent materials are capable of emitting light in the NIR (near-infrared) and visible wavelengths [77]. They can be utilized to compensate for the plasmonic losses in a nano-antenna by non-radiative energy transfer. Referring to the compensation of loss, these materials are also known as gain materials.

Fluorescent dye molecules are small organic chemical compounds, which emit light at visible wavelengths. Some detrimental drawbacks of dye molecules are that they have narrow absorption bands and low optical stability. Figure 5a shows the emission spectra of different dye molecules dispersed in Polymethyl methacrylate with anisole (PMMA A2), (A4 means 2% anisole is used to dilute PMMA) excited at 450 nm and Figure 5b is the prepared solution of those dyes.
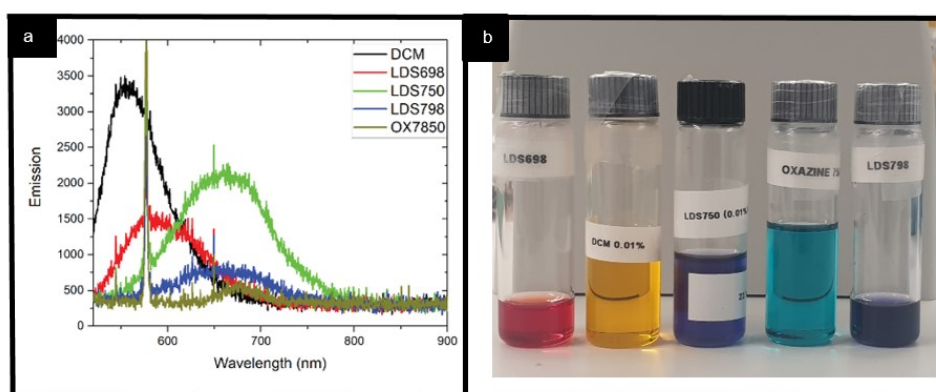
Figure 5.   *a) Emission spectra of DCM, LDS698, LDS750, LDS798, OX750 dye molecules that are excited with a laser at 450 nm. b) Prepared solutions of DCM, LDS698, LDS750, LDS798, OX750 dye molecules with PMMA A2.*
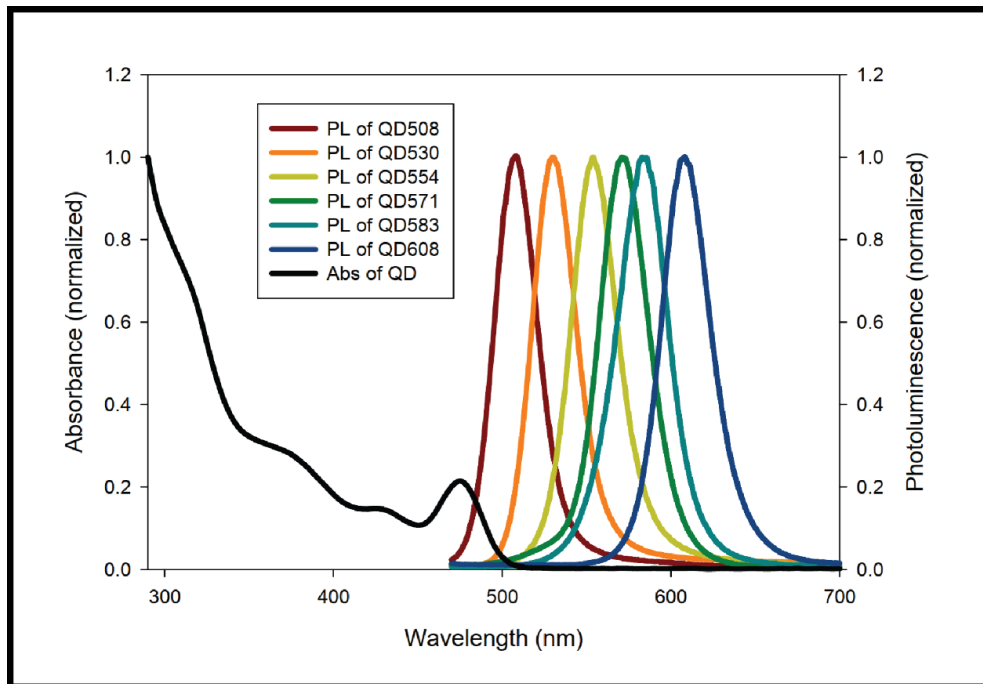
Figure 6.   *Absorption and emission spectra of QD508, QD530, QD554, QD571, QD583, QD608 quantum dots* [78].

Another type of fluorescent material is quantum dots (QDs). These are fluorescent nano-crystal semiconductors. There are core-shell QDs and core-only QDs. Depending on the size and chemical composition, QDs provide a wide range of emission wavelengths [78]. Properties such as high quantum yield, long decay time, size tunability, high chemical and optical stability, broad excitation spectrum, and narrow emission spectrum enable QDs as good candidates for emission studies [79]. Especially, decay time and quantum yield are essential parameters in determining the appropriate fluorescent materials for energy transfer between an emitter and a nanoantenna. Figure 6 illustrates the absorption and emission spectra of QD508, QD530, QD554, QD571, QD583, QD608 quantum dots [78].

2.2.2 Decay time and quantum yield of a fluorophore

The population dynamics of a fluorophore can be described by a two-level model, where the electrons are excited from the ground state by photon absorption. The decay of the populated excited-state is expressed by the following formula,

$$\frac{dn(t)}{dt} = \left(\Gamma_{r,0} + k_{nr}\right)n(t), \tag{2.5.2}$$

where $n(t)$ is the number of electrons in the excited state at time t , $\Gamma_{r,0}$ is the radiative decay rate and k_{nr} is the non-radiative decay rate. The exponential decay of the intensity is given by,

$$I(t) = I_0 \exp\left(-\frac{t}{\tau}\right), \tag{2.5.3}$$

where I_0 is the intensity of emission at time $t = 0$ and τ is the lifetime of the fluorophore which is defined as

$$\tau = \frac{1}{\Gamma_{r,0} + k_{nr}}. \tag{2.5.4}$$

The lifetime can also be calculated by taking the time average of the fluorophore that remains in an excited state. It is defined by averaged time-weighted over the intensity decay of the fluorophore [73]:

$$<t>= \tau = \frac{\int_0^\infty t\, I(t)dt}{\int_0^\infty I(t)dt} = \frac{\int_0^\infty t \exp\left(-t/\tau\right) dt}{\int_0^\infty \exp\left(-t/\tau\right) dt} \tag{2.5.5}$$

Sometimes the fluorophore decays with different lifetimes, multi-exponential decay is used to determine the average lifetime and the photoluminescence decay curve contains multiple exponentials.

Quantum yield (quantum efficiency) of a fluorophore is defined by the ratio of the number of emitted photons, to the absorbed photons. The quantum yield ranges between 0 and 1.

$$\phi = \frac{Number\ of\ photons\ emitted}{Number\ of\ photons\ absorbed} \tag{2.5.6}$$

This expression can be written in terms of the decay rates as,

$$\phi = \frac{\Gamma_{r,0}}{\Gamma_{r,0} + k_{nr}}. \tag{2.5.7}$$

The radiative decay rate is related to the photon emission and non-radiative decay rate corresponds to the sum of internal conversion, external conversion, intercrossing, vibrational and rotational relaxations. It also occurs due to photochemical decomposition, and energy transfer resulted from near field dipole-dipole interactions. From Equations 2.5.4 and 2.5.7, the radiative and non-radiative decay rates can be written as,

$$\Gamma_{r,0} = \frac{\phi}{\tau}, \tag{2.5.8}$$

$$k_{nr} = \frac{1 - \phi}{\tau}. \tag{2.5.9}$$

The radiative decay rate can be modified by controlling the energy transfer process and emission enhancement of the fluorophore. The more emissive fluorophore is denoting higher quantum yield. By calculating the absorption spectra, extinction coefficient and emission spectra of the fluorophore, the quantum yield of fluorophore can be determined.

2.3 Metal-enhanced fluorescence

The incident light at a proper wavelength can excite a chromophore, resulting in the fluorescence process. In fact, excited fluorophore acts as an small oscillating dipole antenna in which radiates emission into far-field. A part of the emitted photons by fluorophore can be absorpbed radiatively by the lossy metal.
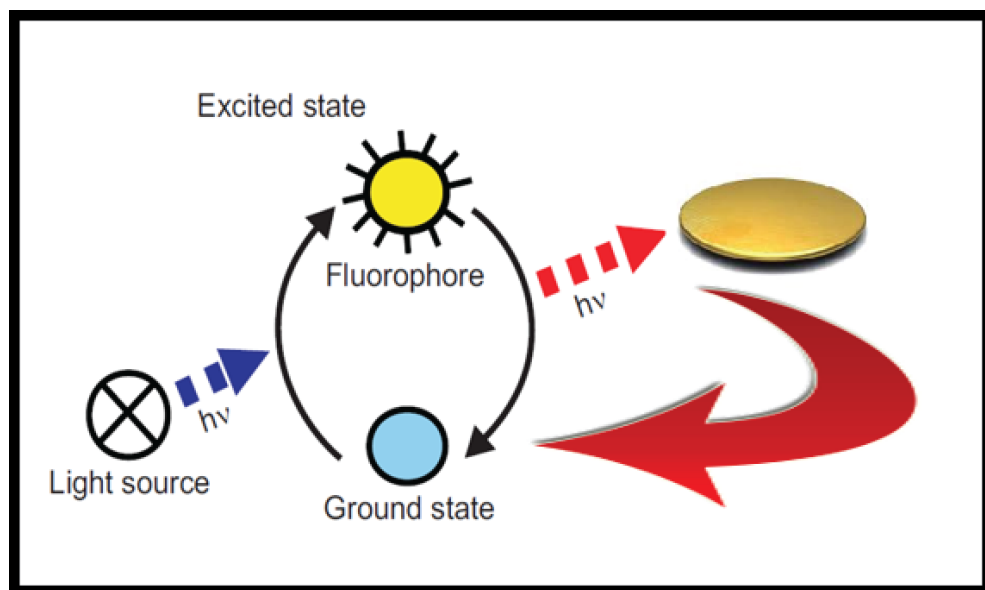
Figure 7.   *Energy transfer between fluorophore and NDs. Dash red arrow toward metal NDs (golden colour disk) shows non-radiative energy transfer and red arrow towards the ground state indicates excitation of fluorophore because of the enhanced local field of NDs.*

On the other hand, the energy of an excited QE (dye molecules, QDs, etc) present in close vicinity of a plasmonic system, can be transferred non-radiatively to plasmonic modes. This can result in inducing oscillating dipoles (plasmons) (Figure 7) and hence the confinement of the electric field around the plasmonic nanostructure. Such localized field can interact with both excited and non-excited emitters, resulting in quenching or enhancing the radiative decay rate. Enhancement of fluorescence in the presence of a metallic nanostructure is called metal-enhanced fluorescence (MEF) [80]. Generally, the emission intensity depends specifically on two main factors; the excitation rate k_{exc} and the quantum yield Φ_E of the chromophore. The emission intensity can be express as

$$I_{PL} = k_{exc}\, \Phi_E. \tag{2.5.10}$$

The excitation rate of an emitter exposed by the local field of a plasmonic nanostructure can be enhanced (lightning rod effect), if the the absorption spectrum of the emitter overlaps with plasmon band of the nanostructure [81]. In this case, the plasmonic structure works as a receiver nanoantenna which promotes much more efficiently the electrons from the ground state to the excited state. This results in emission enhancement, without changing the quantum yield or lifetime of the fluorescent material [73]. Figure 8 shows how the locally enhanced electric field of a plasmonic nanoantenna provides an additional term for excitation rate (E_m), resulting in an enhanced absorption rate. On the hand, when the emisison spectrum overlaps with plasmon band of the nanostructure, the quantum yield of the emitter can be enhanced as a result of the interaction between the local field of plasmonic structure and excited QE. This can be explained by considering the metallic nanostructure as an efficient antenna that out-couples the photons to the far field as a result of the energy transfer to bright plasmonic modes. Another prespective to explain this phenomenta is through the Purcell factor enhancement, which happens due to the increase in optical density of the states and hence decreasing the modal volume of the nanostructure [81]. Such decrease in effective cavity modes can increase the radiative decay rate of the QE, which changes the quantm efficiency and lifetime parameters. The modified lifetime and quantum yield of the QE placed in close proximity of nanostructure can be expressed as

$$\tau = \frac{1}{\Gamma_r + k_{nr} + k_{ET} + \Gamma_m}. \tag{2.5.11}$$

$$\phi = \frac{\Gamma_r + \Gamma_m}{\Gamma_r + k_{nr} + k_{ET} + \Gamma_m} = (\Gamma_r + \Gamma_m) \times \tau. \tag{2.5.12}$$

k_{ET} stands for the non-radiative energy transfer from the QE to plasmonic antenna which acts as a new channel to modify the non-radiative decay rate of the emitter [82]. As a result of this, the intrinsic radiative decay rate ($\Gamma_{r,0}$) of the emitter modifies to Γ_r (quenching effect). Based on equation (2.5.11) these modifications shorten the lifetime of the QE. Γ_m is the introduced enhancement in the radiative decay rate by the plasmonic nanoantenna (see Figure 8). It is evident from equation (2.5.12) that the quntum yield can be enhanced if the weight of the enhancement in radiative decay rate would be higher than the weight of the shortening in lifetime [83]. In contrary, the overall effect will be the quenching of the emission, even if the radiative decay rate is enhanced. Thus, the observed quenching in the emission of a QE in vicinity of a plasmonic system can be explained in two ways; first the nanradiatvie energy transferred mostly to "dark plasmon modes" which dissipate the energy through the ohmic losses of the metal. Second, as it

is mentioned, the transferred energy to "bright plasmon modes" are not that much prouned as compared to transferred energy to dark modes [84]. This happens mainly because the emitter and plasmonic dipoles radiate out of phase, hence their EM fields interference destructively. Consequently, the total dipole moment decreases which results in reduction of both absorption rate and radiative decay rate.
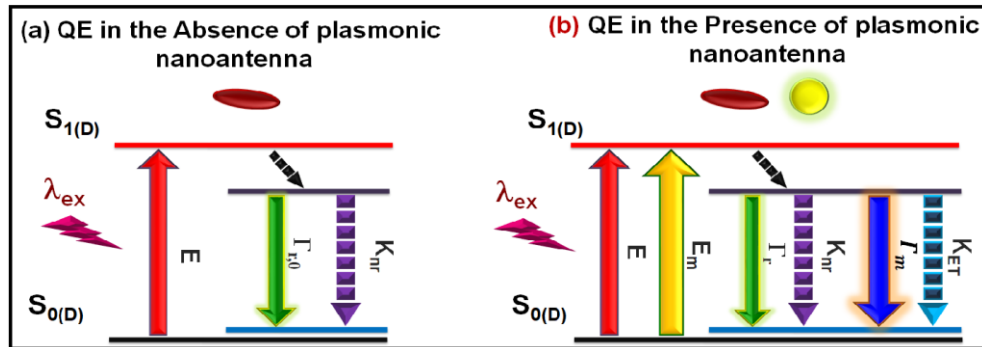
Figure 8.   *Jablonski diagram for a) the fluorescence of a QE in the absence of plasmonic nanoantenna and b) the process of the excitation enhancement and emission enhancement of a QE due to localized electric field of plasmonic nanoantenna and for new decay channels .*

2.4 Spontaneous emission modification in the plasmonic hybrid system

A resonant cavity with overlapping mode with the resonance of a quantum emitter can modify the spontaneous emission of the emitter and the local density of photonic states of the cavity. This effect is known as the Purcell effect [85]. Before Purcell, this spontaneous emission was known as an intrinsic radiative property of the molecules. Purcell's work established on this concept that if an electric dipole is placed in a resonant cavity; the spontaneous decay rate of the dipole is enhanced compared to the free-space decay rate [63]. The occured coupling regime can be determined by comparing the field-emitter coupling constant with the photon decay rate in a cavity (Γ_r) and the non-radiative decay rate (k_{nr}). The coupling constant is

$$\chi = [|\boldsymbol{d}|^2 \frac{\omega_0}{2\hbar\varepsilon_0 V}]^{1/2}, \tag{2.6.1}$$

where ω_0 is the frequency corresponding to the energy separation between excited and ground states of the emitter, $\boldsymbol{d}$ is the dipole moment of optical transition, V is the resonator effective volume, e is the electron charge, and ε_0 is the vacuum permittivity. In the weak coupling regime, $\chi \ll \Gamma_r, k_{nr}$, which means that the hybridization between the emitter and the resonator is weak [86]. In this regime, the decay rate of the QE can be achieved by the Purcell factor which depends on two important quantities; the quality factor and the modal volume of the resonant cavity [87].

$$F = \frac{3}{(4\pi^2)} \left(\frac{\lambda_0}{n}\right)^3 \frac{Q}{V} \tag{2.6.2}$$

where $\frac{\lambda_0}{n}$ is resonance wavelength in the system surrounded by QEs. The Purcell effect can be expressed in terms of the decay rate of the emitter near the resonator (Γ_r), and the one in free space ($\Gamma_{r,0}$) [55],

$$F = \frac{\Gamma_r}{\Gamma_{r,0}} = 1 + \frac{6\pi\varepsilon_0}{|\boldsymbol{d_1}|^2} \frac{1}{q^3} \Im[\boldsymbol{d_1}^*.E_s(\boldsymbol{r_d})]. \tag{2.6.3}$$

Here $\Gamma_r = \frac{\omega_0^3 |\boldsymbol{d_1}|^2}{12\pi\varepsilon_0 \hbar c^3}$, $\boldsymbol{d_1}$ being the dipole moment of the dipole oscillating with frequency (ω_0), q is the wavenumber in free space, $E_s(\boldsymbol{r_d})$ Is the secondary local field at the emitter position. In Equation 2.6.3, $\Gamma_{r,0}$ expression does not present the non-radiative decay (because $\Gamma_{r,0} \gg k_{nr}$). The radiated power by the dipole $\boldsymbol{d_1}$ at a frequency (ω_0) can be calculated as follow

$$P_{0,rad} = \frac{\omega_0^4 d_1^2}{12\pi\varepsilon_0 c^3}. \tag{2.6.4}$$

and

$$\Gamma_{r,0} = \frac{P_{0,rad}}{\hbar\omega_0}. \tag{2.6.5}$$

Here, Γ_r is the ratio between $P_{0,rad}$ and photon energy. During the coupling, only the radiative power is modified by the environment. We can write a modified decay factor as

$$\Gamma_{r,0} = \frac{P_{rad} + P_{nonrad}}{\hbar\omega_0}. \tag{2.6.6}$$

So, the Purcell factor based on the power can be obtained from 2.6.5 and 2.6.6 as;

$$F = \frac{\Gamma_r}{\Gamma_{r,0}} = \frac{P_{rad} + P_{nonrad}}{P_{0,rad}} = F_{rad} + F_{nonrad}. \tag{2.6.7}$$

Here, P_{rad} is far zone radiated power and surrounding environment enhanced it, while P_{nonrad} is lost power in the environment.

If we have the lossless electromagnetic environment, no energy is dissipated in the surrounding environment ($P_{nonrad} = 0$). So, the change of the total radiative power can be described by the Purcell factor at the frequency of the emitter as following [85].

$$F = \frac{\Gamma_r}{\Gamma_{r,0}} = \frac{P_{rad}}{P_{0,rad}}. \tag{2.6.8}$$

where subscript zero refers to radiative power of the same emitter in free space. This assumption is applicable to most of quantum dots and fluorescence dye molecules [85]. In our studied system, this equation is used to calculate the Purcell factor by using the ratio of power radiated by the emitter in the presence of the plasmonic nanodisk and the

absence of nanodisk. Equation 2.6.8 assumes that the non-radiative losses inside the emitter are negligible.

Purcell factor can be significant with those nanoantennas which allow optical radiation of quantum source by converting it to the near field. An effective nanoantenna should have a tunable cross-section and provide considerable local field enhancement. The local field around a plasmonic nanoantenna arises as a plasmon mode, and it can be used with the plasmon hybridization with emitter and nanostructure [63]. In the presence of nano-antenna, spontaneous emission of the hybrid system can be enhanced significantly, a demonstration of which is the main objective of this study. The coupling between nano-antenna and QE modes depends on the absorption spectrum of the nanoantenna and emission spectrum of the fluorescence. This energy transfer can be considered similar to the energy transfer from a fluorophore as a oscillating dipole, to the plasmonic reso-nator as another dipole, [82]. The emission enhancement factor is described as

$$\gamma_{Em} = \frac{C_{sca}}{C_{sca0}}. \tag{2.6.9}$$

Here γ_{Em} is the enhancement factor, C_{sca} and C_{sca0} are the total scattering cross-section in the presence, and absence of the nanoantenna, respectively [37]. Emission enhance-ment of the fluorophore depends on the coupling with the plasmon mode, which can be controlled by the size of the nanoantenna. Based on the emission wavelength of the fluorophore, one can determine an appropriate shape of the nanoantenna to tune the plasmon resonance.

3. METHODS

In this chapter, the numerical and experimental methods that have been used to investigate the coupling between plasmonic NDs and quantum emitters are introduced. Earlier studies showed that the opticalproperties of NDs are affected by their geometry [71]. In this sense, the energy transfer between NDs and quantum emitters is investigated using ND arrays with different size and periods.

The design of the NDs and optimization of the resonance wavelengths are based on the numerical simulations. The designed NDs are fabricated using e-beam lithography nanofabrication technique. The fabricated NDs are characterized to obtain their optical response as well their interaction with the quantum emitters.

The chapter is organized as follows. We first present the details of the numerical simulations. Then the fabrication process is explained in detail. And finally, we present the characterization methods.

3.1 Design and Simulations:

The design of the nanoantennas (nanodisks) are based on the solutions of the full-wave Maxwell's equations by finite difference time domain (FDTD) method [88]. This method is used to determine the coupling of the penetrating field through the structure. FDTD method is advantageous in numerical analysis, as it works in the time domain allowing simulations within an extended range of wavelengths without requiring excessive computational time and power. This method is based on the direct solutions of Maxwell's curl equations. It is modelled by using a cubic unit cell space lattice (Figure 9) where Maxwell's equations are implemented. The properties of the electromagnetic wave are obtained by this model when it propagates into a space of specific volume, containing a conducting structure or dielectric. The incident wave propagates within the structure, and this is tracked by time-stepping in each cell of the space lattice. During the interaction surface-current, penetration, diffusion, diffraction is tracked within the time for each lattice cell. This whole method is achieved by analyzing the small portions of the propagating wave along with the structure (unit cell), which interacts with the wave front at a given instant in time [88].
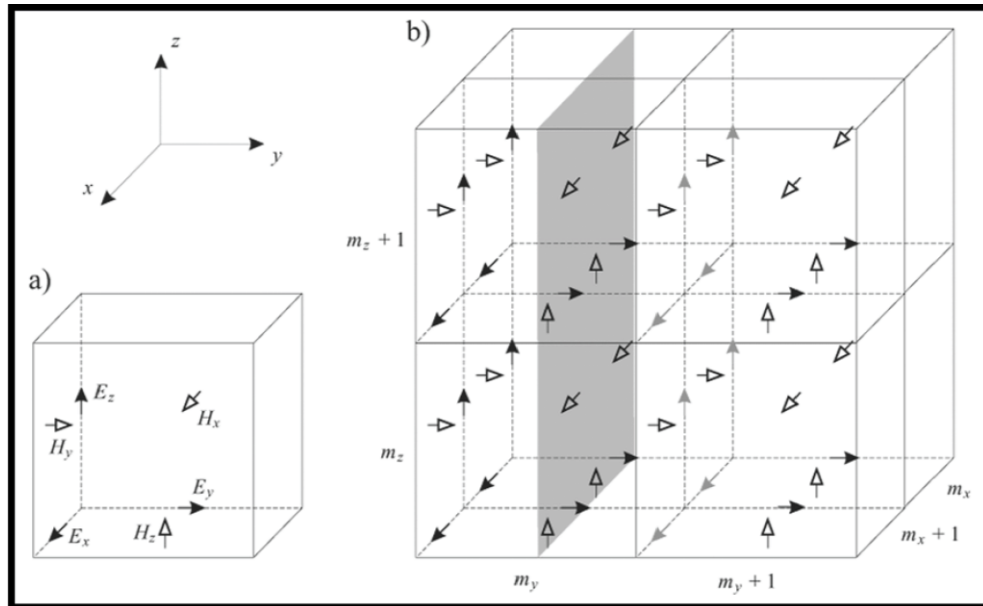
Figure 9. *a) FDTD lattice cell: solid and hollow arrows indicate the electric and magnetic field components, respectively. b) This is a demonstration of the total field/scattered field boundary. Black shaded surface is the equivalent surface which is normal with the y-axis. Gray arrow is the modified electric field* [89].

As in Figure 9, cubic cell space lattice contains the electric field and magnetic field, which are positioned along the axis. FDTD method is based on the surfaces or the interiors of the dielectric or conductive structures. The boundary condition is used for vanishing the tangential component of the electric field and normal component of the magnetic field of the surface, which shown in Figure 9 (b) [89,90].

A commercial software, *Lumerical* FDTD Solutions™ has been used to simulate the reflection, transmission and near field profiles of NDs arrays with different sizes and periodicities. Besides, we calculate the Purcell factor of a dipole emitter to understand the interaction of the nanoparticle and the quantum emitter.

3.1.1 Reflection, transmission and field profiles

We optimize the nanodisk array in terms of the substrate, the size of the nanodisks, and the array periodicity, based on the reflection calculations. The reflection maximum of each sample is the localized plasmon resonance of the nanodisk array. We have used two different substrates, which are SiO_2 (glass) and Si-SiO_2. In Si-SiO_2 the thickness of the SiO_2 is 280 nm. The optical properties of the Si and SiO_2 are modelled in Lumerical FDTD Solutions by using experimental data from Palik model [91]. Gold (Au) is modelled using the experimental refractive index data provided by Johnson and Christy model [92]. The thickness of the nanodisks is 70 nm, and the diameter vary between 105-195 nm, for the period of 360 nm, 400 nm, and 440 nm.

We simulate the one-unit cell of the periodic nanodisk array (See Figure 10) by employing periodic boundary conditions in the directions parallel to the light propagation. The boundaries perpendicular to the light propagation is set perfectly matched layers (PML). We added a mesh overwrite region enclosing the nanodisk, with mesh size 3 nm. The source is a broadband plane wave source within the range 500-1000 nm, which is normally incident at the nanodisk array and propagates along the axes of the nanodisk from air to substrate. A 2D power monitor is located behind the source plane to collect the reflected light having the same wavelength range as the source. Another 2D power monitor is located over the nanodisk to record the near electric field profile at the desired (resonance) wavelength for each sample. The power monitors collect the power and display the powers, normalized to that of the incident field by default. Therefore, our reflection results are obtained out of 1, where 1 corresponds to the case of a total reflection, and field profiles show the intensity enhancements near the nanodisks.
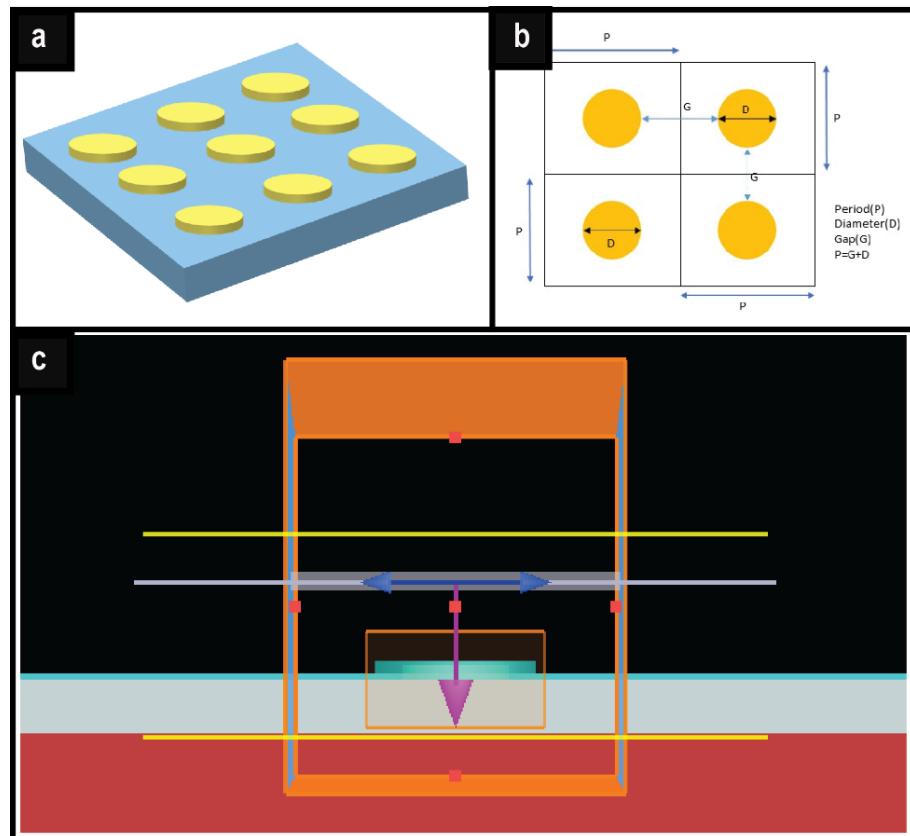
Figure 10. *a) Nanostructure scheme with height 70 nm, diameter 140 nm and a period of 360 nm. b) Design parameters of nanodisks diameter (D), gap (G), period (P). c) The unit cell of NDs extracted from Lumerical FDTD Solutions . The circular object inside the green layer is ND. The thin green layer is a PMMA layer. The pink arrow is the plane wave incident on NDs. The yellow line above this is for reflection, and the bottom one is for transmission monitor (used for transparent sample). Box around the NDs is fine mesh area.*

After running simuatons for different periods and diameters, the effect on the resonance peak is observed. Figure 10b shows the parameters considered in the simulations. The period, the diameter, and the gap between the NDs is changed step wisely to have an optimized design. Figure 10c shows the simulation unit cell with the power monitors, transmission monitor, source and boundary around the unit cell.

3.1.2 Purcell factor calculations

In the Purcell factor calculations, a quantum emitter is modelled as a dipole source that is located at the hot spot of the NDs. First, electric field profile of the NDs with a broad-band plane wave source is simulated to extract the hot spot, and then the maximum intensity spot is determined as the location of the dipole source with emission wavelength set to the resonance wavelength of the NDs. We perform the Purcell factor calculations for all possible orientations of the dipole emitter. Average Purcell factor is calculated based on the position and orientation of the dipole around the NDs. Figure 11 shows the simulation region of the Purcell factor calculations, with the dipole position with respect to NDs. In Figure 11, only parallel orientationed dipole with respect to NDs is shown.
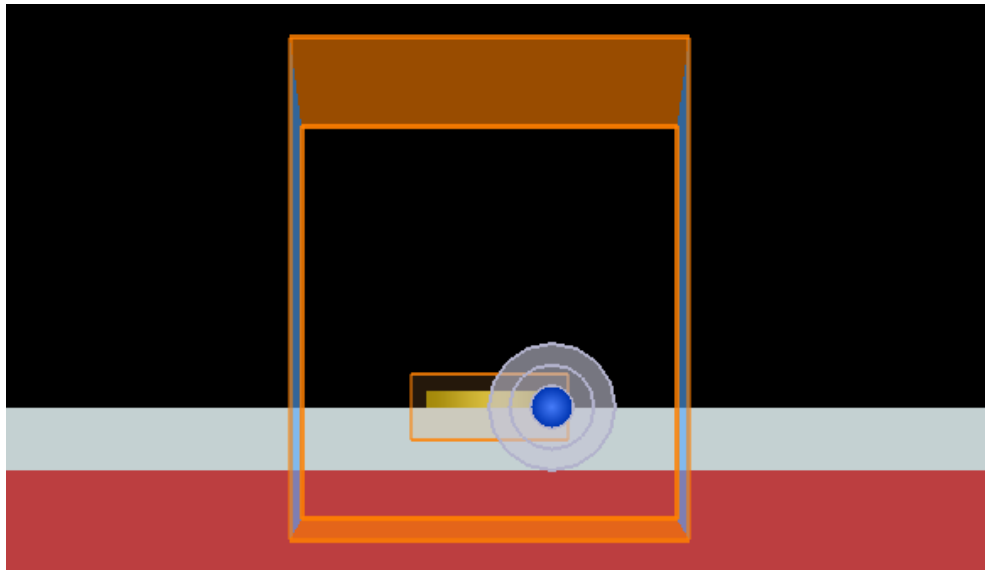
Figure 11. *The golden colour object is NDs and dipole source (Blue circle) placed in the hot spot of NDs electric field for Purcell factor simulation.*

3.2 Fabrication

The optimized nanodisk arrays are fabricated by electron beam (e-beam) lithography technique. In this section, the details of the whole nanofabrication process are given, including spin coating, e-beam lithography for patterning, e-beam evaporation for the

deposition, lift-off process for obtaining the final samples, and finally the SEM for the imaging of the samples.

3.2.1 Spin-coating

Spin coating is a method which is used to deposit uniform thin films of coating materials on top of a flat surface [93]. In this process, coating material placed on top of the sample with low spinning or without spinning. After dropping materials, the sample is rotated with high speed, which ensures that the material spreads uniformly on top of the sample by centrifugal force [94]. The speed is determined based on the material data sheet and the desired thickness value. The thickness of the film is determined by the material viscosity, concentration of the solution, and the solvent that is used to dissolve it. Usually, solvent evaporation determines the final thickness of the film. Evaporation temperature is deter-mined based on the evaporation temperature of the solvent [93,95]. After spin coating, samples are baked to evaporate the solvent.
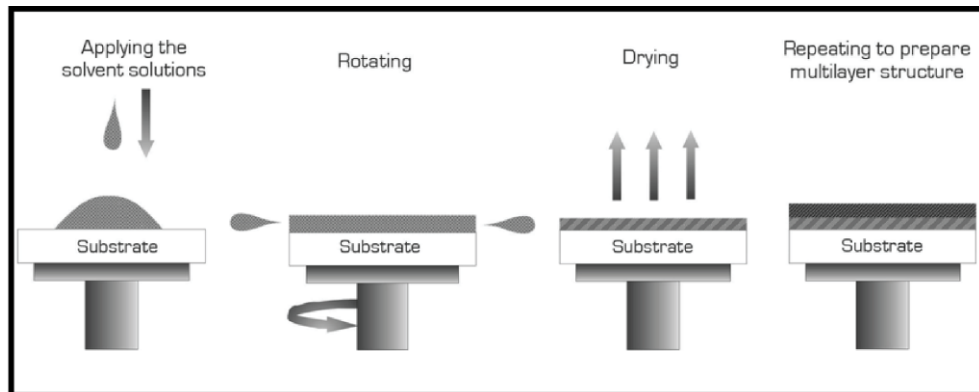
Figure 12.   *Spin coating method for depositing the thin film.* [96].

Figure 12 represents the spin coating process. This process is used before lithography to spin coat PMMA on top of the substrate (the parameter used in this process will be explained in the next section). After spin-coating on a substrate, the substrate is ready for e-beam lithography to make the pattern. The spin-coating process is also used to add dye+PMMA layer on top of fabricated NDs.

3.2.2 E-beam lithography:

In this technique, a focused beam of electrons scans a surface which is covered by an electron-sensitive film, called resist, to obtain custom patterns [97]. The beam alters the solubility properties of the resist material, which enables removal of either exposed or non-exposed parts of the resist by immersing it in an appropriate solvent afterwards. It

is a powerful technique, allowing one to obtain structured surfaces in the nanometer scale, with less than 10 nm resolution [98]. There are several steps to follow for fabrication, which are summarized in Figure 13, and each step is essential for proper structure patterning. The type of resist material, exposure dose, and e-beam spot size are considered for optimizing the development of the nanostructure after patterning. The thickness control of the resist is based on the spin coating and the type of resist.
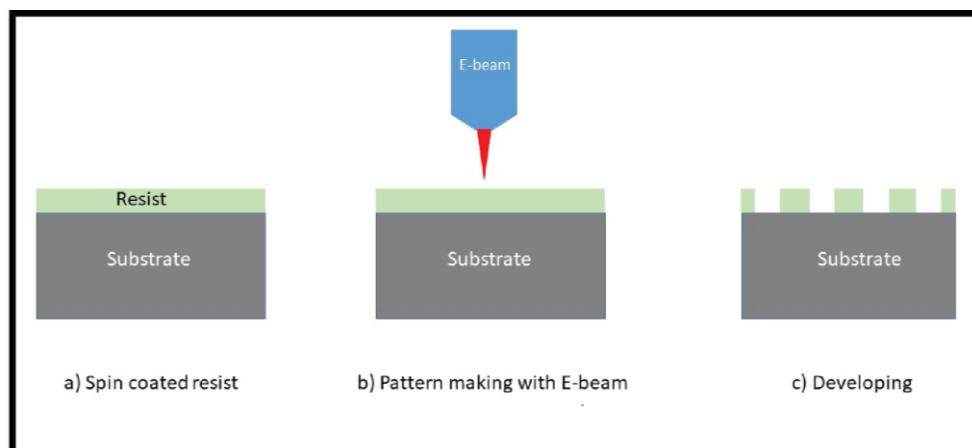
Figure 13.   E-beam lithography diagram.

We use PMMA A4 950 as the resist material. The resolution limit of the EBL is high by using PMMA and dense array nanostructure is possible with PMMA. The substrate is spin-coated with 3000 rpm (revolutions per minute) for 40 s and baked in 180^0 C, to have a 250 nm thick resists layer. A conductive polymer (aquaSAVE) is also coated on the sample with the same rate. In pattern making, 600X magnification is used with a working distance of 4 mm. Value of EHT (electron high tension) is 20 kV, and the writing field is 100×100 micron for each matrix, and the aperture size is 10 microns. The sample is exposed to e-beam with a dose of 300 $\mu C/cm^2$. Different dose parameters result in different sizes of nanodisks, which eventually provides the desired diameter.

To develop the patterned structure, 1:1 of IPA and MIBK is used as developer and IPA as stopper before moving the sample for metal deposition. Sample in IPA and MIBK is kept for 60 s while in IPA for 30 s to finish the development process.

After pattering, we use the e-beam evaporation for the deposition of Au over the pattern. The working principles of e-beam evaporation and the parameters used in the nanofabrication is discussed in the next section.

3.2.3 E-beam evaporation:

Figure 14 illustrates the working principle of the e-beam evaporation technique. The bottom part of the equipment has a crucible, which contains the deposition material (Au).

The material is evaporated from the crucible to the sample by being exposed to the electron gun. The whole process is in a vacuum environment, and the sample is placed precisely on top of the crucible. Based on the desired thickness, the deposition rate needs to be controlled. Use of quartz crystal is vital for controlling current and voltage, which controls the deposition rate. A proper deposition rate is required to achieve a uniform layer of metal over the substrate or pattern substrate [99,100].
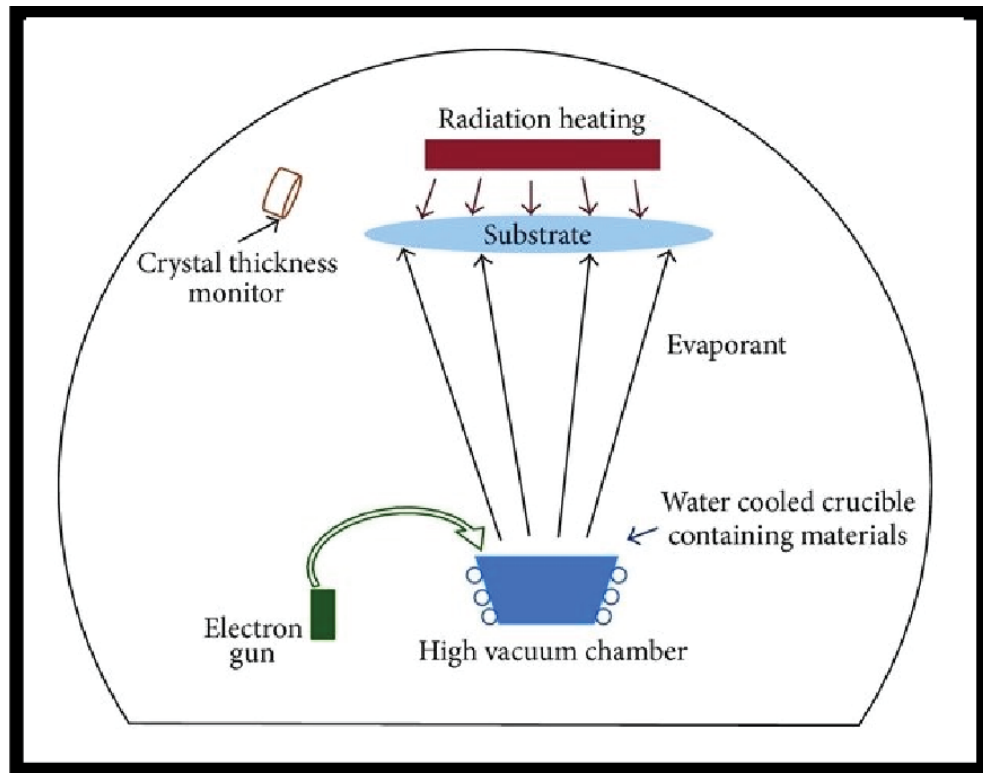
Figure 14. *Schematic of the e-beam evaporation instrumental setup for deposition of metal.* [100]

After obtaining the patterned resist by the e-beam lithography, we deposit the desired metal by e-beam evaporation. Our patterned sample is coated with 70 nm of Au. The deposition is done with a constant rate of 1 A^0/sec. The pressure and operating voltage are 9×10^{-6} mBa and 7.28 kV, respectively.

3.2.4 Lift-off

Lift-off is the process where the resist is removed, and the final form of the samples are given. In this work, acetone is used as a lift-off medium in the sample preparation process. Acetone removes the unexposed-PMMA with Au on top of it. Au layer that is directly deposited on the substrate by using a resist mask stay after lift-off [101,102]. After 24 hours of lift-off process, the structure got its final shape. After the lift-off process, the

size of the NDs is measured by SEM (Scanning Electron Microscope). SEM process is briefly discussed in the following section.

3.2.5 SEM (Scanning Electron Microscope)

SEM is an electron microscope, which produces images of the samples by scanning the sample surface with a focused beam of electrons [103]. SEM has a higher resolution compared to an optical microscope because the wavelength of the electron is 10^5 times shorter than the visible light wavelength.
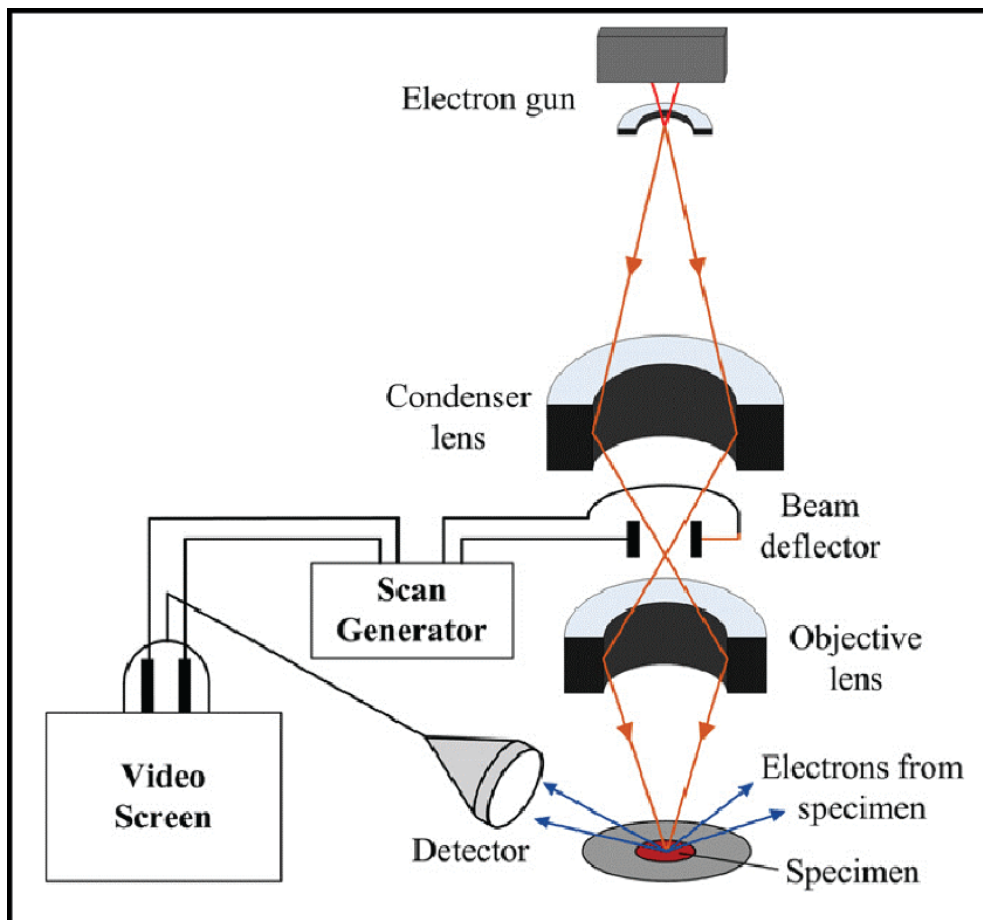
Figure 15. *Schematic diagram of the SEM where it shows how the electron beam hits the sample and detector collected the electrons* [104]*.*

As schematized in Figure 15, the electron gun emits electrons towards the sample, under the acceleration voltage, which passes through the condenser and the objective lens. It forms a beam of electrons with a few nanometers in diameter. When this beam hits the specimen surface, it produces an electron signal which is collected by the detector and converts it into an image point. The image points are formed based on the number of electrons detected from corresponding points on the specimen and displayed in the video screen [104,105]. The electrons collected during the interaction of electron beam and

specimen surface are Auger electrons, secondary electrons, reflected electron, transmitted electrons, characteristic X-rays, absorption electrons, Cathodoluminescence (CL) [106] (Figure 16).
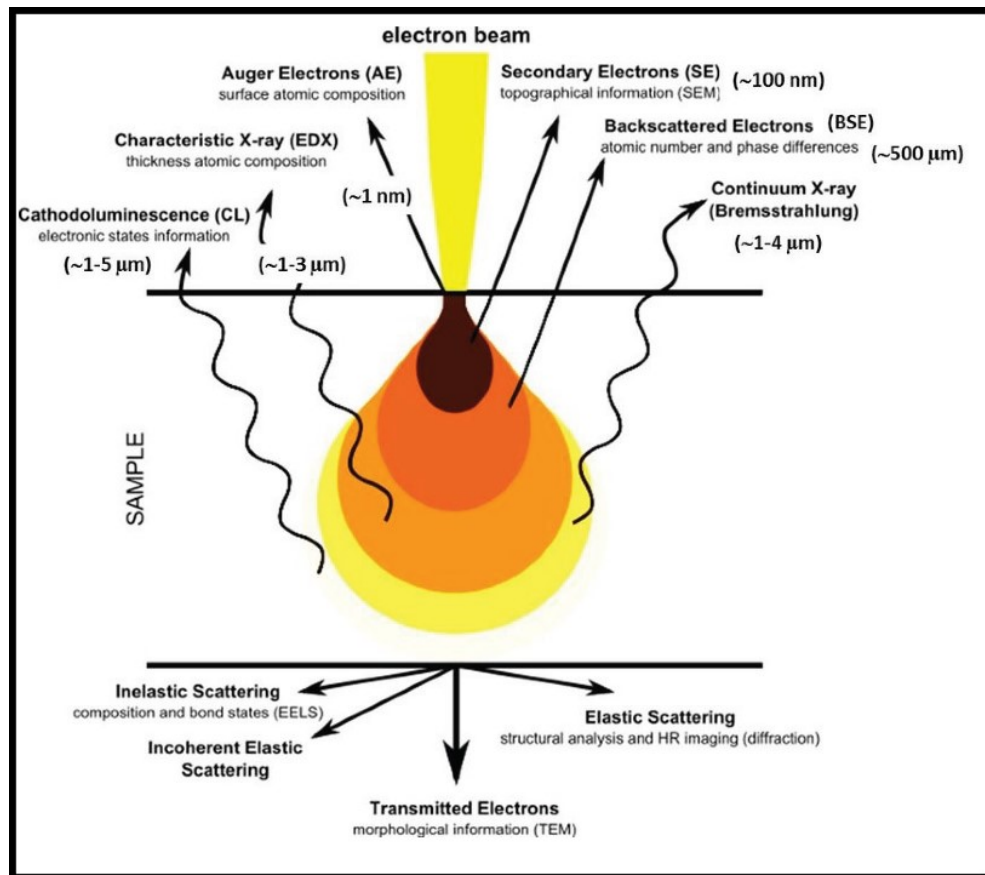
Figure 16. *The energy of total electron beam light after interaction with the sample emitted with the different signal from the parts of the sample surface* [106].

Monitoring the interaction of electrons with the atoms of a sample provides information about the topography of the surface and its composition. This method can provide an image of the sample surface with a very high resolution (less than 1 nm).

The diameter and periodicity measurements of ND samples are taken by the SEM (Carl Zeiss Pvt. Ltd) equipment with 1kx magnification power and 1nm resolution.

3.3 Sample preparation

After fabricating the nanodisk, proper dye selection is necessary for this experiment. Based on the simulations, different dye solutions are prepared to check their extinction and emission. PMMA A2 is used to vary the density or concentration of dye molecules. The mass percentage is the main parameter for the dye solution. The formula 3.1 is used for the mass concentration

$$Mass\ percentage = \frac{Mass\ of\ dye}{Mass\ of\ (dye + solvent)} \times 100\% \tag{3.1}$$

Molarity of the solution can also be calculated from the solution preparation by equations 3.2 and 3.3 as follows,

$$Molarity\ (M) = \frac{dye\ in\ molar\ mass}{solvent\ in\ litre} \tag{3.2}$$

$$Molarity\ (M) = \frac{Mass\ of\ dye}{Molar\ mass\ of\ dye} \times \frac{1}{\frac{Solvent\ volume\ in\ ml}{1000}} \tag{3.3}$$

The solution prepared for measurements is in units of mass. Equation 3.4 is used to convert it to units of volume as follows,

$$Solvent\ volume\ in\ ml = \frac{Mass}{Density\ of\ the\ solvent} \tag{3.4}$$

DCM, LDS 698, LDS 750, LDS 798, Oxazine 750 perchlorate dye solution with PMMA A2 is prepared for the emission and extinction measurement. We spin-coated the solution on the nanodisks with the recipe of 4000 rpm for 40 s. They are then baked in a hot plate at 150℃ for 90s. Then this sample is ready to observe the emission enhancement. By changing the mass percentage of the dye, we can control the number of dye molecules that interact with the nanoantennas. It is not possible to obtain reasonable results with too high or too low concentrations of dye molecules in PMMA A2. The discussions regarding getting the optimum concentrations are given in the 4th chapter. The thickness of the dye molecules solution on the nanoantenna varies based resist type and speed of the spin coater.

3.4 Measurement setup

The characterization of the nanofabricated samples is based on absorption, reflection, and photoluminescence measurements. The laboratory (Metaplasmonics Lab, Tampere Uni.) that we used to characterize the samples is equipped with confocal microscopy (provided by WiTec - alpha 300 series), a schematic of which is given in Figure 17. This microscopy offers the opportunity to do the following experiments:

1) Static spectroscopy
    - Absorption and reflection measurements
    - Photoluminescence microscopy
2) Pump-probe confocal microscopy
3) Time-resolved fluorescence spectroscopy

4) Raman spectroscopy
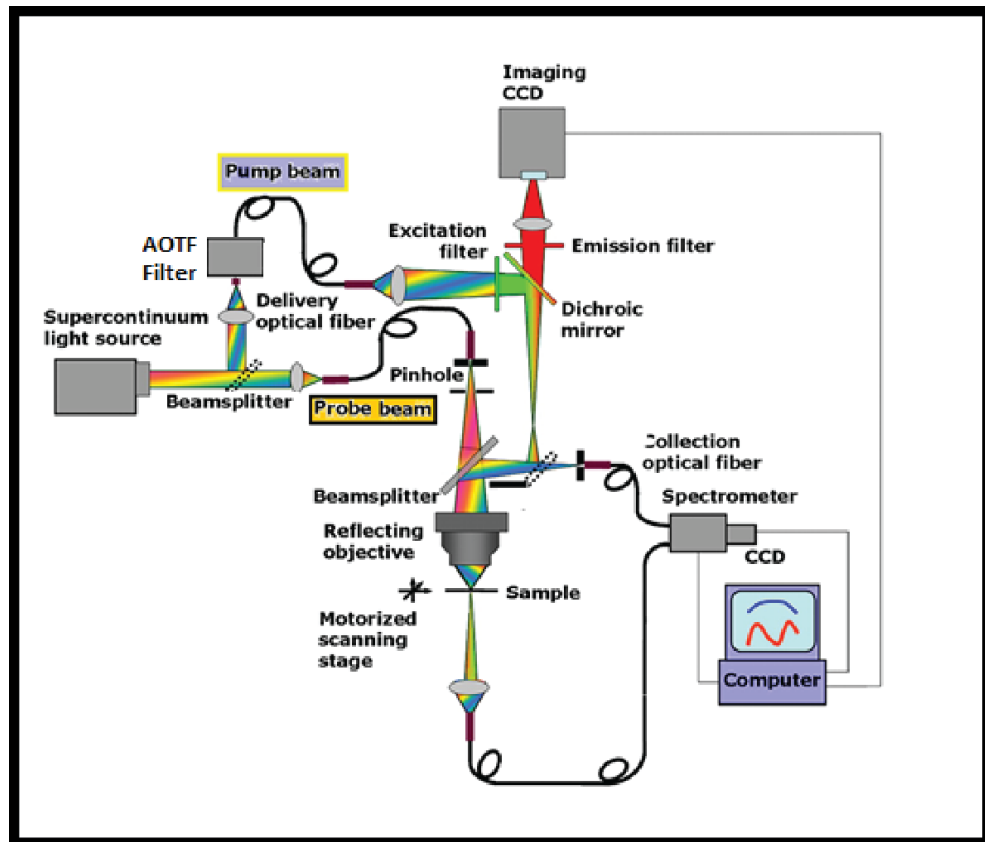
Figure 17. *Schematic of multi-functional spectroscopy setup from WiTec and light source is a supercontinuum laser.*

The detector, which works in the visible range, can be used both for reflection and transmission measurements. We have a CCD detector from WiTec and Ocean Optics (Flame) for our experiment. For nanodisk sample measurements, a white light source (supercontinuum Fianium laser), and green laser (532nm) are used. We can mount an optical fibre in the coupler to use different sources. AOTF (acoustic-optic tunable filter) gives us the freedom to choose the wavelength from the continuum laser. Measurement of the sample by using the above system is explained in the following sections.

3.5 Characterization of the plasmonic response

We first measure the reflection spectra of the ND samples to determine the plasmon resonances. Then, the absorbance and emission bands of different dyes are measured to determine which dye molecules would be proper for further experiments.

For the reflection and transmission measurements white light source and Fianium laser are used. For the reflection measurements, first reference reflection from Al reflector is

taken. After background calculation, reflection from the NDs is taken. By the following equation, the reflectance is calculated

$$Reflectance\ (\%) = \frac{Reflection\ (NDs) - Background}{Reflection\ (Al) - Background} \qquad (3.5)$$

For the transmission measurement, first reference transmission from the substrate is taken, and later transmission from the NDs is obtained for transmittance. Transmittance is calculated by using the same equation 3.5, where reflection (NDs) is replaced by the transmission and the reflection (Al) by transmission (glass). These experiments are repeated for the bare sample and sample coated with PMMA to observe the resonance shift. During all these measurements 50X objective, and a natural density filter 3 for reflection (2,5 for transmission) are used. Natural density filter is used to reduce the intensity of the white light source because, without the filter, the signal saturates the detector.

Absorbance of the dye molecules obtained via transmission measurements. The drop casted dye on top of a glass slide used to measure the absorbance of the dye molecules. However, it is not possible to measure the absorbance on the non-transparent sample. Hence, the transmission and absorbance of the NDs on glass substrate are measured.

Furthermore, emission of the dye molecules is measured using 532 nm continuous wave laser excitation. Based on these measurements and analyses, LDS750 dye is selected as the appropriate quantum emitter for this work. Dye concentration preparation is discussed in the section 3.3 (sample preparation).

3.6 Characterization of the plasmon-emitter coupled response

Fianium pulse laser with tunable repetition rate is used to excite the dye because it is possible to select the wavelength based on the absorption of the dye. It also gives us the flexibility to change the power of the laser by changing the repetition rate and its percentage of illumination. Emission experiment of dye molecules spin-coated NDs sample shows the plasmon-emitter coupled response, which is going to discuss in the following section.

3.6.1 Emission measurement

For emission experiment, CW (continues wave) laser is used with excitation wavelength of 532 nm to excite the dye spin-coated NDs sample. Notch filter (535 nm) is used to block the excitation from the spectrum. To compare the emission intensity change, we have taken emission of dye molecules in the absence and presence of NDs, as showed

in Figure 18. In this experiment, Fianium laser (532nm) is used with a repetition rate of 5 MHz with the power of 100 uW. Objective 50x is used with an integration time of 500 ms for this whole emission experiment.
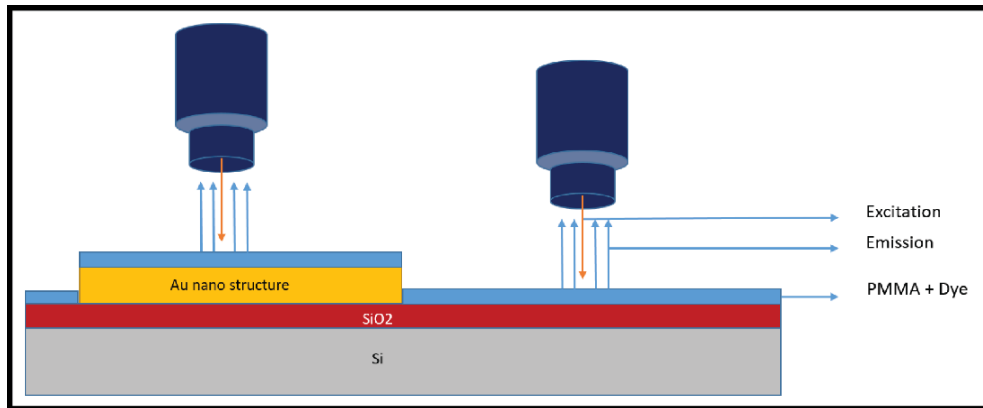
Figure 18. *Representation of excitation and emission measurement setup of an NDs sample. The yellow line shows the laser or lamp incident light on the sample, and the blue line shows the reflected light.*

3.6.2 Lifetime measurement

For lifetime measurements, we used Pico-quant system integrated to our microscope. The HydraHarp 400 is the time-correlated unit from Pico-quant, and SymPhotime software is used to collect the data.

Figure 19 represents the working principle of Time-Correlated Single-Photon Counting (TCSPC) unit. Pulse laser is used for excitation and condition of the system adjusted so that at least one photon reaches to detector per laser pulse. As shown in Figure 19, Δt is calculated by measuring the time between the excitation pulse and observed photon. This time difference saves as a form of the histogram, which shows the data as the decay of the waveform. Constant function discriminator (CFD) is used to measure the time of the pulse and time to amplitude converter (TAC) is used to convert the signal to a voltage [73].
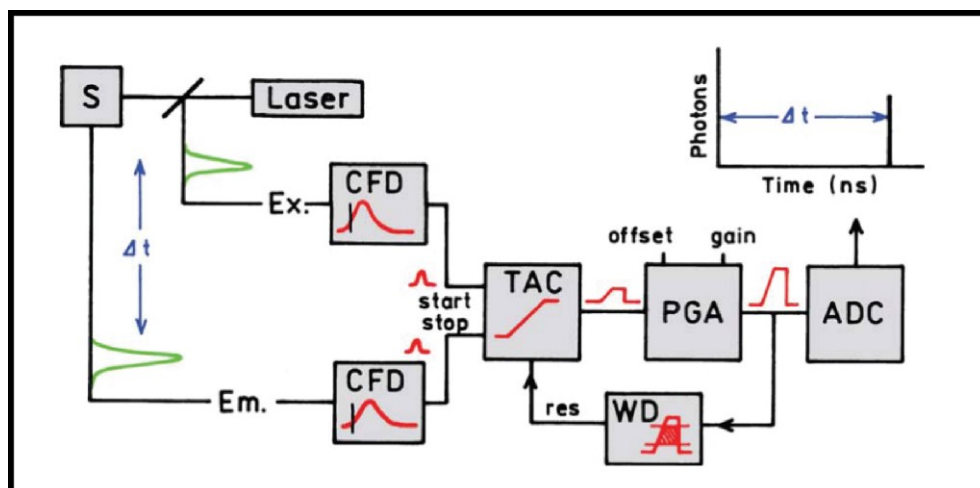
Figure 19. *Schematic of the TCSPC (Time-Correlated Single-Photon counting)* [73]*.*

Note that, we have two different configurations for lifetime measurement 1) WiTec system and 2) Pico-quant system. In our lifetime experiments, we used Pico-quant system with Fianium laser for excitation at 532 nm wavelength along with the repetition rate of 10 MHz. The photon collection time is kept as 20 s in the whole experiment. The laser is coupled with Raman coupler, which has a notch filter of 535 nm, which blocks the incident light wavelength. APD (avalanche photodiode detector) is used for detection.

3.6.3 FLIM (Fluorescence-lifetime imaging microscopy)

In the last characterization, FLIM technique is used with WiTec system and APD. FLIM is based on the excited state decay differences of the dye on a different part of the sample. This image gives the information of the contrast based on the lifetime of the specific dye, not the emission spectra. Repetition rate 20 MHz (at 532nm) is used with an integration time of 10 ms for large area scan. This measurement gives the information of the dye on that area through counts, lifetime which can analyse through the WiTec software. FLIM techniques are classified as time domain and frequency domain. In our experiment, time-domain FLIM with TCSPC is used. Figure 20 summarizes the working principle of the FLIM used in this work.
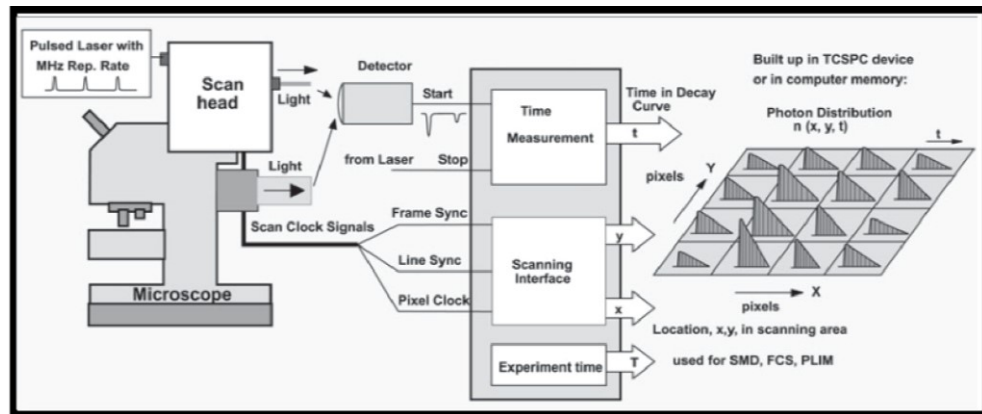
Figure 20. *Schematic of the TCSPC FLIM* [107]*.*

In FLIM measurements, sample scanned by the pulse laser beam. The detector detects the photons of the fluorescence light from the sample surface and determining the time difference between laser pulse, the arrival time of the photons. In addition, the position of the laser beam on top of the sample during photon detection also recorded to provide whole FLIM measurement. The image is the result of 2D (2 dimensions) area scan with 3D (3 dimensions) data from each pixel which contain photons in a large number in time bin. In Figure 20, pixels show the decay rate in each pixel for the whole image and the entire image is the photon distribution on the scanned surface. This image contains a total photon number with wavelength and time data [107]. Photon distribution over the x and y corrdinates are recorded based on the times of the photons.

4. RESULT AND ANALYSIS

The main aim of our systematic study is to investigate the interaction between plasmonic NDs (nanoantennas) and LDS750 fluorescent dye molecules for spontaneous emission enhancement. Figure 21 shows the SEM images of the fabricated nanodisks with electron beam patterning method (for details see method section).
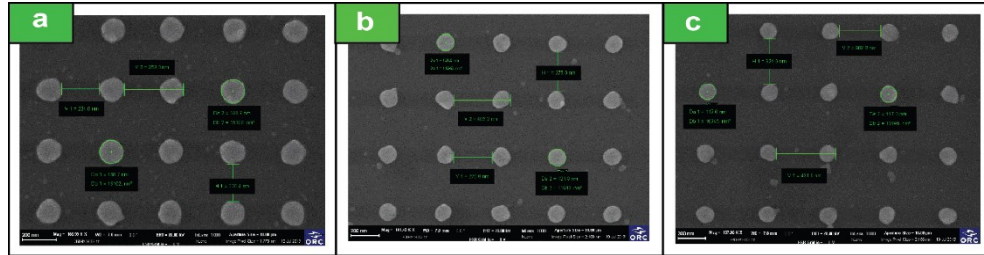
Figure 21. *SEM images of fabricated NDs sample of a) 360 nm b) 400 nm and c) 440 nm period.*

Figure 22a demonstrates the resonance band change in the reflection spectrum for samples with similar diameter but different period. The resonances are weakened and red-shifted by the increase of the period. When the period increases, the number of NDs on beam spot decreases which reduces the total electric field confinement in the illuminated part; as a result, intensity drops. Local field of NDs changes by the change of period because the local field interaction changes as the gap get larger through the increase of period. So, the increase in the period shifts the resonance to higher wavelengths. Experimental results in Figure 22a also agree with this argument.

4.1 Environment effects on NDs Plasmon resonance

The substrate effect indicates the dependence of nanostructures optical properties to the external dielectric environment [50]. Figure 22b shows the simulation and experimental results of the NDs on top of $Si - SiO_2$ and the glass substrate. In these results, the surrounding environment is air (n=1). A proper substrate should be selected by considering two facts: the operational range of the experimental setup in the visible range and the availability of a fluorescence dye molecules with proper emission peak in the preferred range. Based on the acquired experimental and simulation results, we observed that high refractive index of the substrate shifts the plasmon resonance to higher wavelengths. In another study, by discrete dipole approximation method, it is also shown the effect of

substrate refractive index on the plasmon resonance [9]. After the analysis of the measurements and simulations, $Si - SiO_2$ is chosen as the substrate for further experiments in this thesis.
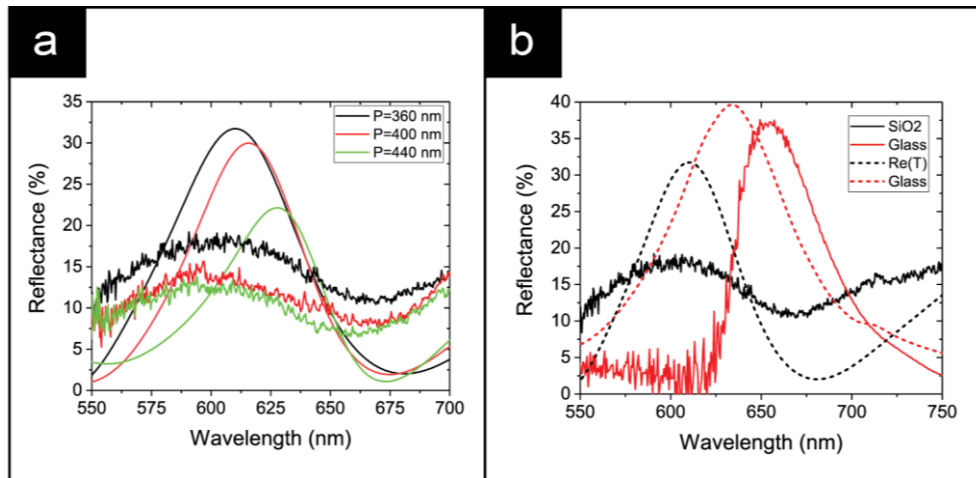
Figure 22. *Simulated and experimental reflection data of 130 nm diameter NDs for a) different periods on $Si - SiO_2$ substrate, b) different substrates for period 360 nm.*

Figure 23 illustrates this environment effect on the plasmon resonance. First, the reflection spectrum of NDs is acquired while they are exposed directly to the air. Afterwards, the same NDs are spin-coated with 50 nm thick layer of PMMA. Changing the environment from air to PMMA (n=1.48) red-shifted the resonance band between 40-60 nm. The dielectric constant for the metal in equation 2.1.15, shows that the plasmon frequency of nanoantennas varies with the refractive index of the environment because the refractive index is related to the dielectric function as follows $\varepsilon_d = n^2$ (ε_d is used instead of ε_o because the medium changed from air to PMMA). Here n is the refractive index of the dielectric medium. Therefore, plasmon resonance is red-shifted by the increase of the refractive index of the environment.

As PMMA used as the homogenous host medium for dye molecules, the spectral overlap between the resonances of the NDs and emission of the dye molecules is considered while NDs are covered by PMMA. In Figure 23 (a-d), the spectra of the 360 nm period NDs are presented in both environments of air and PMMA. In lower diameter (range 105-155 nm), we observed a red-shift around 40-50 nm, while for diameters bigger than 155 nm the shift increases to 60 nm. These measurements are done by WiTec confocal microscopy in reflection configuration with Fianium pulse laser in the broadband mode as a light source. After studying the environmental effects, the size dependency of NDs plasmon resonances with three different periods is numerically and experimentally investigated.
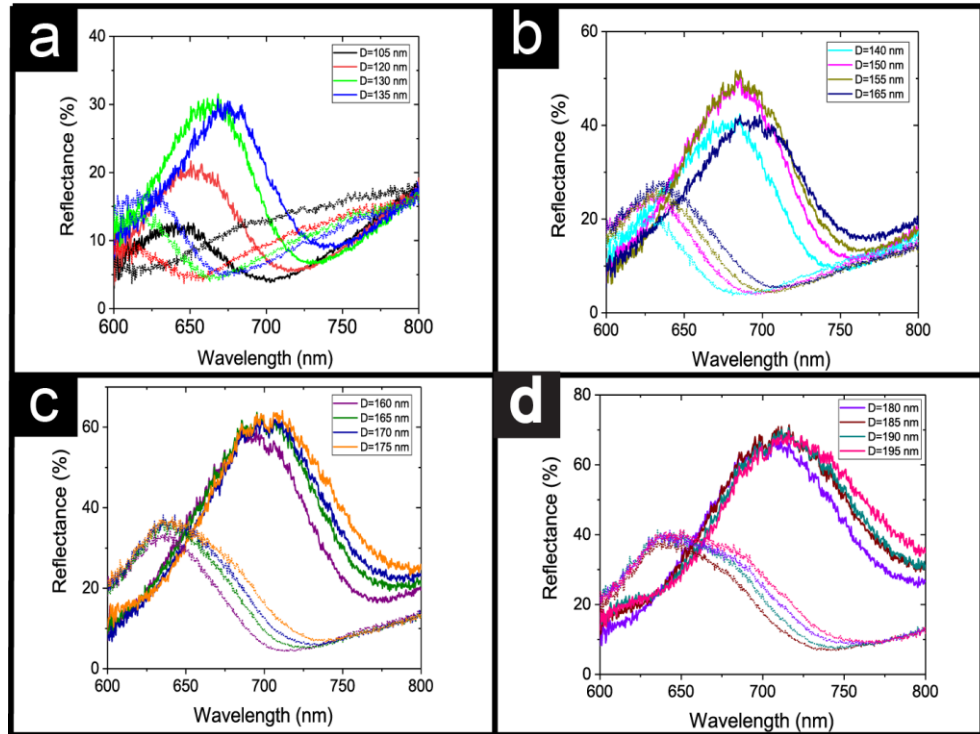
Figure 23. *(a-d) Experimental reflection results of 16 different samples with diameters from105-195 nm and a period of 360 nm. Same colour represents the same diameter of NDs with and without PMMA, more reflective results are for NDs with PMMA (redshifted in all NDs).*

4.2 Plasmon resonance dependence on diameter and period

Plasmon resonance of the NDs depends on their size and period of NDs array. It can be tuned by changing either diameter or period or by a simultaneous change of these two parameters. Tuning the plasmon resonance helps to achieve a better spectral overlap in hybrid plasmonic systems. Figure 24 demonstrates the simulation and experimental reflectance results of NDs for period 360 nm, 400 nm and 440 nm with different diameters. For a specific period, the shift of the resonance band to higher wavelength is evident while the nanoantennas diameter increases. However, the intensity and the peak position of the shifted resonance are different, as the period is changed. From Figure 24, it is clear that by increasing the NDs diameter, the bandwidth of the resonance increase, whereas the quality factor decreases. The incident light is normal to the sample, and the same objective is used to receive reflected light in all these experiments. After measuring the plasmon resonances of NDs, as it is explained in the next section, the proper QE with the emission band in the range of 600-700 nm is selected.
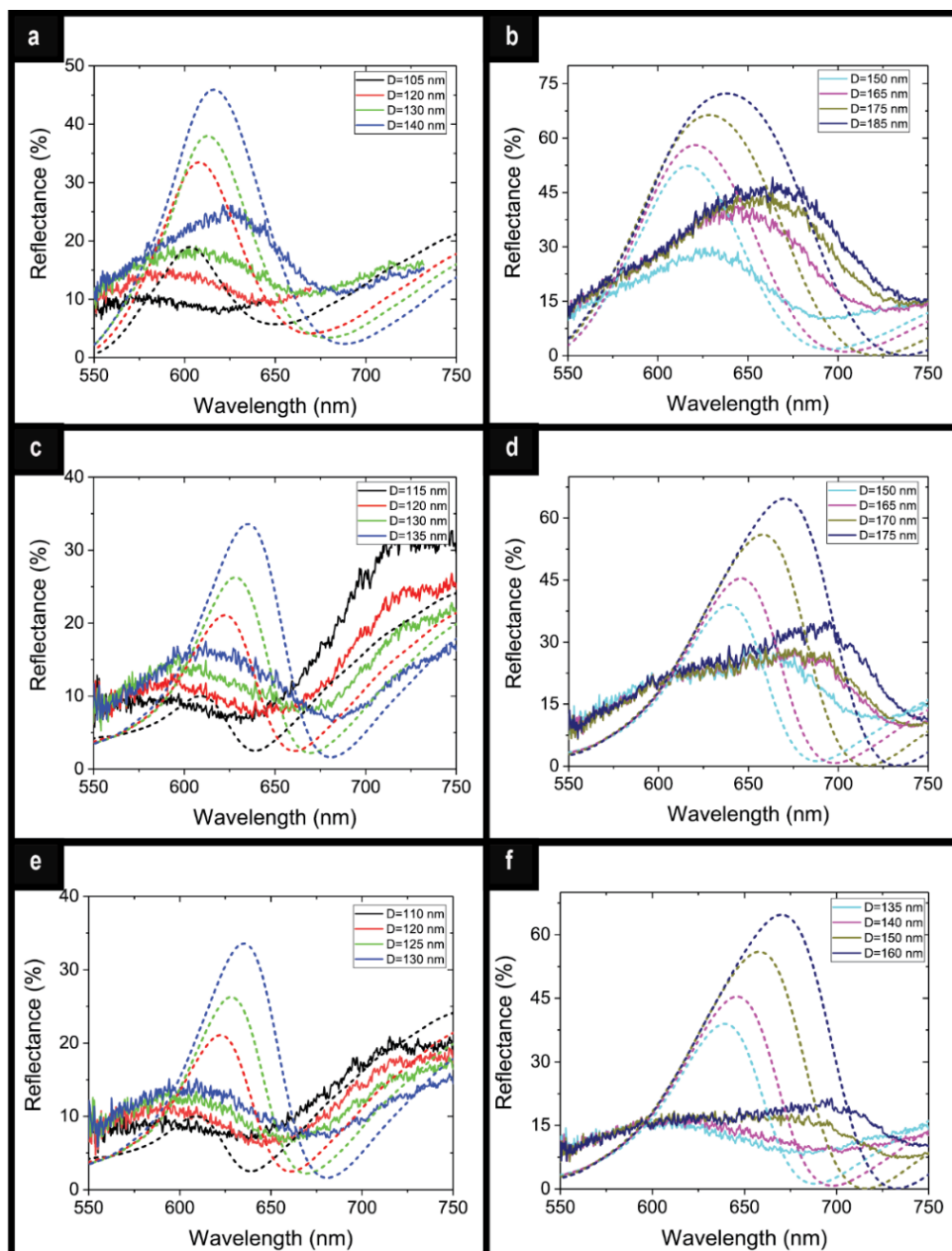
Figure 24. *a), b) Simulation (dashed lines) and experimental (solid lines) reflection results of a sample with different diameter NDs for a period of 360 nm, c), d) 400 nm and e), f) 440 nm.*

4.3 Dye selection for hybrid plasmon system

To select a proper QE, extinction and emission of different fluorescent dye molecules such as DCM, LDS698, LDS750, LDS798, Oxazine750, homogeneously dissolved in PMMA A2 are acquired. These mixtures are spin-coated on top of a fused silica substrate at 4000 rpm for 40 sec and later baked at 150 °C for 90 sec. For extinction experiments, broadband laser-driven light source (Energetiq), operating in the range of 170-2100 nm is used. The excitation light is coupled by fibre to the confocal microscope, which is configured in the transmission configuration.
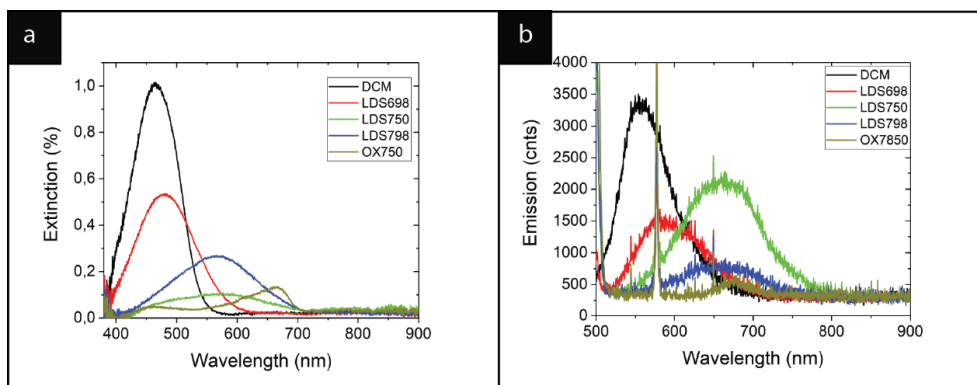
Figure 25. *The figure presents the extinction (a) and emission band (b) of DCM, LDS698, LDS750, LDS798, Oxazine 750. These dyes spin-coated on top of the glass substrate.*

Figure 25a shows that each of these dye molecules has a different extinction band. Based on these results, the best excitation wavelength for each of the dye molecules can be selected individually. By providing the proper excitation energy, higher than the bandgap energy of the QEs, the electrons in the ground state absorb the excitation light and promote to the excited state. After undergoing some non-radiative processes, the excited electrons populate the lowest excited electronic state. The relaxation of the molecules from this state to the ground state can be accompanied by emitting photons (photoluminescence). It is expected that the dye molecule with stronger absorption results in a higher emission for the same intensity of the excitation source. But this is not always true since the quantum efficiency of different dyes is the main parameters which determine the intensity of the dye emission. In Figure 25b, emission spectra of the dye molecules are illustrated. For the emission measurements pulse laser (Fianium) operating at 480 nm with the repetition rate of 5 MHz is used, and a long-pass filter of 500 nm is used on detection path to block this excitation wavelength. As it is evident, only LDS750, LDS798 have the emission band in the range of 600-700 nm which overlaps with the resonance band of the designed NDs. However, since LDS750 with emission peak at 650 nm, has higher emission intensity (higher quantum efficiency), we selected this dye as the best candidate to investigate the emission enhancement of QEs by our designed nanoantennas.

4.4 Emission enhancement of dye in hybrid plasmon system

A 50 nm layer of gain media embedded in PMMA polymer remains on top of the nanoantennas after evaporating the anisole by baking the sample. We need to take it into account that before the spin-coating active layer of PMMA, 5 nm Al_2O_3 is deposited over on top NDs by ALD (Atomic layer deposition) technique. This thin layer works as the

spacer between plasmonic antennas and the dye molecules in order to prevent direct charge transfer which results in quenching of the gain material radiative decay rate [108].

The spectral overlap between the reflectance of NDs and the emission band of LDS750 in the case of different diameters for the periods of 360 nm, 400 nm and 440 nm are shown in Figure 26. As it is shown, the reflectance of NDs with lower diameters (105-140 nm) is in the left side of LDS750 emission band. For the diameters equal or bigger than 150 nm related to the arrays with the periods of 360 and 400 nm, the resonance bands efficiently overlap with or shift to the right side of the emission band. We observe a better spectral overlap for 440 nm NDs array with 135 nm diameter, while the resonance band of NDs with a diameter bigger than 135 nm moves the right side of the LDS750 emission band. However, NDs with a diameter lower than 125 nm have resonances in the spectral range lower than the peak wavelength of LDS750 emission.

It should be considered that because of the environment (PMMA) influence, the resonance bands red-shift about 40-50 nm. As a result of this red-shift, the NDs with resonance band in the left side of the emission spectrum undergoes a better spectral overlap than the NDs with bigger diameters. As the reflectance spectra of all NDs overlap partially or entirely with the emission band, the PL enhancement for LDS750 dye is expected in every case. However, as a result of much efficient spectral overlap for NDs with lower diameter, a stronger emission enhancement is achieved, as compared to the higher diameter ones. The modifications in NDs diameter changes the resonance bands peak position. Moreover, the intensity of the absorbed light is decreased by increasing the diameter.
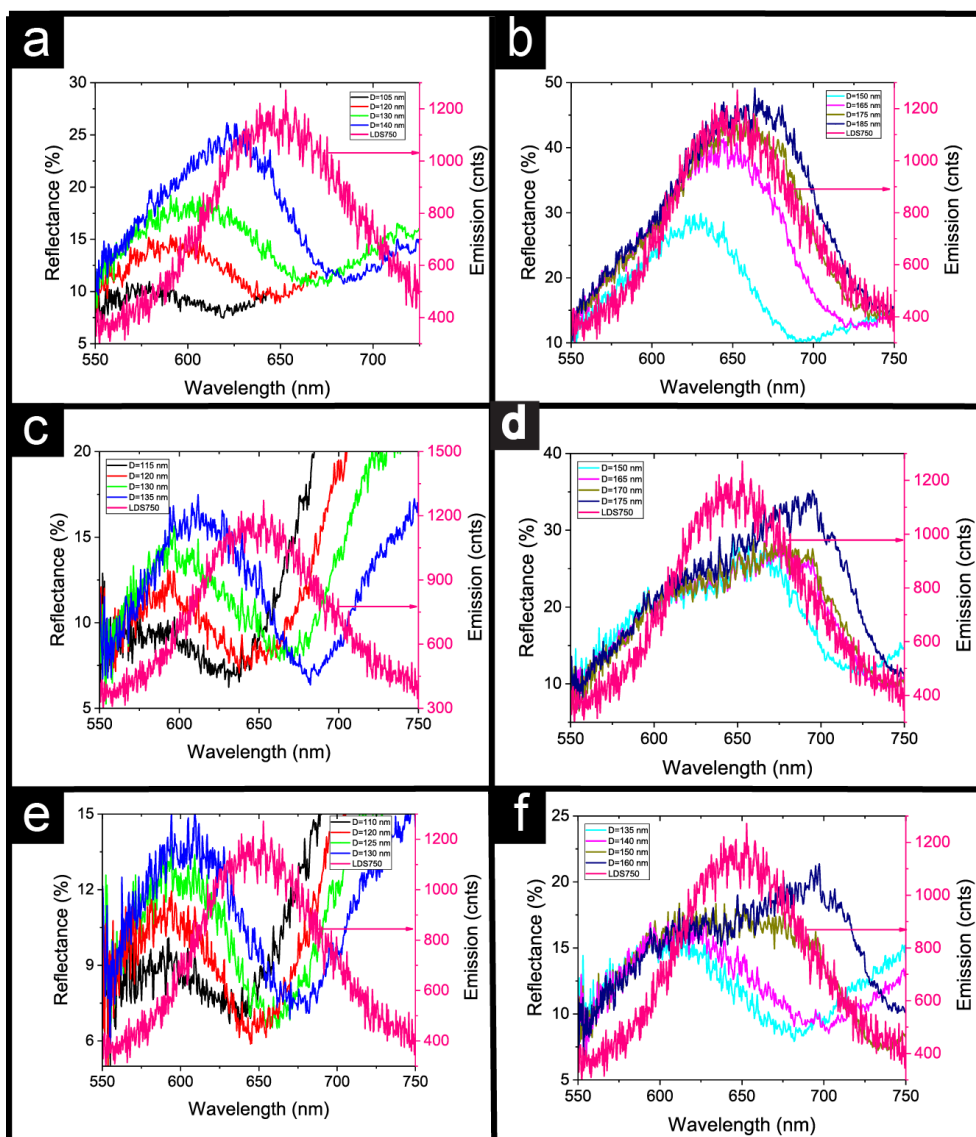
Figure 26. *The overlap of the reflection of NDs and emission spectrum of LDS750 0.01% dye. The left side of the y-axis presents reflectance (black) of the NDs in period 360 nm (a, b), 400 nm (c, d), 440 nm (e, f) and right side of the axis present emission counts of LDS750 dye (pink).*

As it is shown in Figure 26, for the periods of 400 nm and 440 nm, the resonance peak of NDs with the same diameter is red-shifted. This effect modifies the spectral overlap between the NDs resonances and LDS750 emission spectrum. Accordingly, the achieved PL enhancements are different for different periods. The modification of the spectral overlap between the fixed emission peak of LDS750 and NDs with three different periods are observed, while the diameter is fixed. As it is clear from Figure 26, the best spectral overlaps are obtained for NDs with of diameter 140 nm (360 nm period), 135 nm (400 nm period) and 125 nm (440 nm period). The number of homogeneously spin-coated LDS750 molecules in $100 \times 100 \ \mu m$ area of each NDs matrix is 2×10^{12} (Appendix).
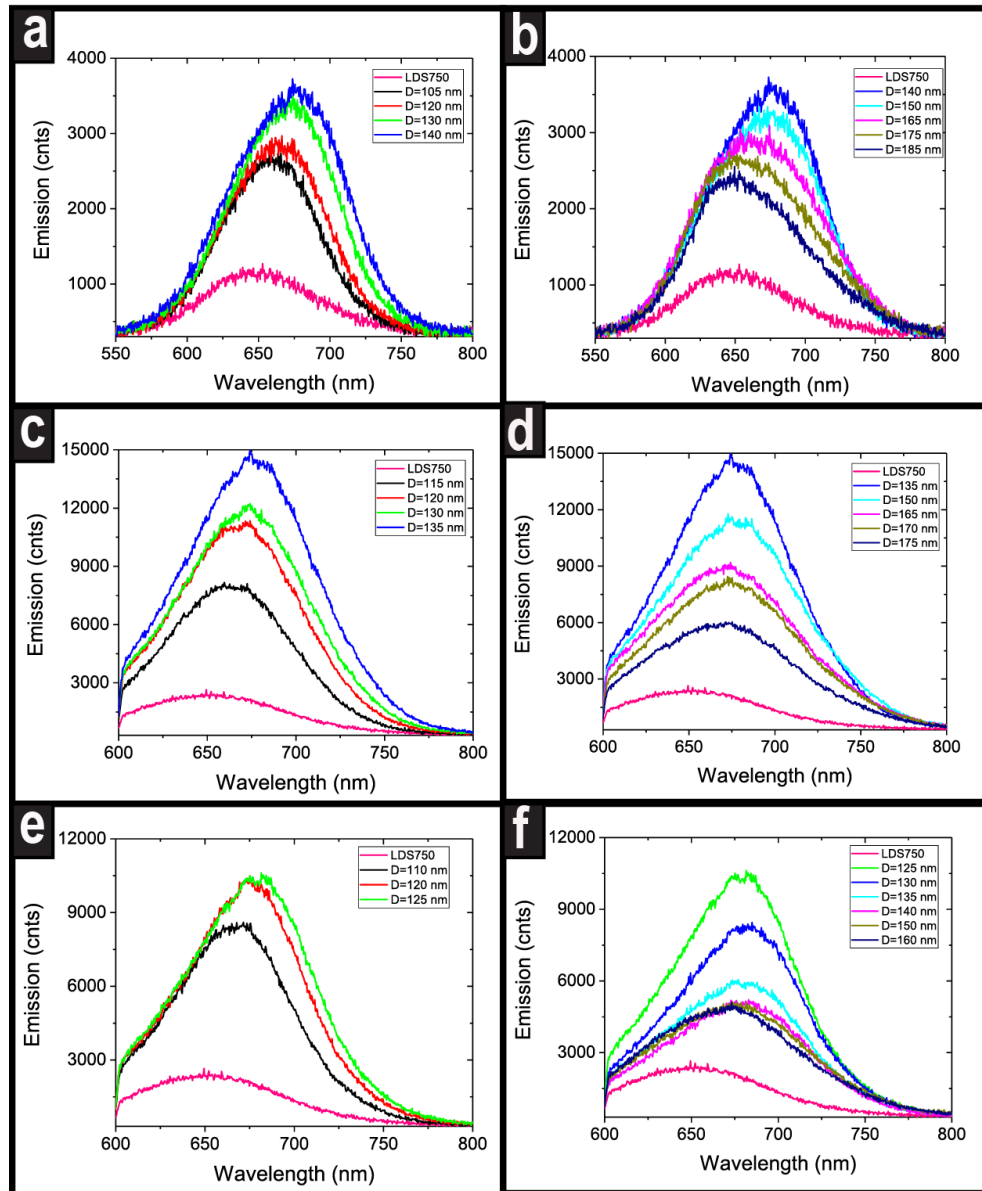
Figure 27. *Emission of dye in the presence and absence of NDs. The pink line shows the emission spectrum of the dye molecules and the others show the spectrum of the emission of dye in (a, b) for the period of 360 nm. (c, d) for the period of 400 nm. (e, f) for the period of 440 nm in the presence of NDs.*

The emission spectrums of dye molecules in Figure 27 are measured by WiTec confocal microscope in the reflection configuration. Excitation source for the emission experiment continues wave laser operating at 532 nm, and long-pass filter of 550 nm is used for the period of 360 nm, while for the period of 400 and 440 nm, 600 nm filter is used. When light hits on the sample surface, it excites the dye molecules. The oscillating dipoles of the dye molecules transfer the energy non-radiatively to plasmonic nanoantennas, which have resonance band overlapped with the emission spectrum of the emitters. The transferred energy enhances the local fields of NDs. Such enhancement can promote more

dye molecules from the ground state to the excited state. The overlap between the electronic excited states of donor and plasmonic acceptors changes as the diameter of NDs changes. This happens as the spectral overlap between the resonance band of NDs with different diameters and emission band of dye molecules changes. By decreasing the overlap of the electronic excited states, the confinement of the local field decreases, which affects the emission enhancement factor of LDS750. By placing the dye molecules in close vicinity of the plasmonic NDs, the excitation rate of NDs can be increased. As a result of the local field enhancement, the modal volume decreases, and consequently Purcell factor enhances. So, in the presence of NDs quantum yield of the dye molecules increases. From equation 2.5.12 we can see that there is a new radiative decay rate related to NDs, which increases the quantum yield. On the hand, for NDs with lower diameters, stronger local field confinement and lower modal volume are expected. These result in the increase of the quality factor of the resonators and therefore enhancement of the Purcell factor. Based on the explained phenomena, our designed NDs work as the receiver antenna. On the other hand, these NDs operates as efficient transmitter antennas. This can be observed as the appeared red-shift in the peak position of the enhanced emission of the dye molecules. As the spectral overlap for NDs with lower diameter gets stronger, the shift of the emission to the higher wavelength is much more pronounced. The observed red-shift is explained by the outcoupling of the plasmons to the far-field by plasmonic nanoantennas. In the array of NDs with 360 nm period, one can say that for diameter of 185 nm, NDs mostly are working as receiver antennas rather than the transmitter ones, while for the diameter of 140 nm, both receiving and transmitting effects are playing a role in the observed enhanced emission.

4.5 PL enhancement factor and power dependence of PL

In the previous section, it is presented that PL enhancement of the dye molecules are changing in different diameter of NDs because plasmon band shifts by changing diameter. Therefore, different PL enhancement factor is observed. Figure 28 shows the calculated reflection of the NDs in 3 periods and these three NDs has close resonance wavelength with different intensity. These three NDs arrays have better overlap with the emission of the dye molecules. The fabricated sample area is 100×100 μm, which means NDs number per sample vary for different periods. As the gap is small in small periods, more NDs fits in the same area, which increases probability more reflection. Electric field profiles in Figure 28(b, c, d) show that the electric field confines around the NDs. In these profiles, the samples with 400 nm, 440 nm and 360 nm have a higher local field in descending order.
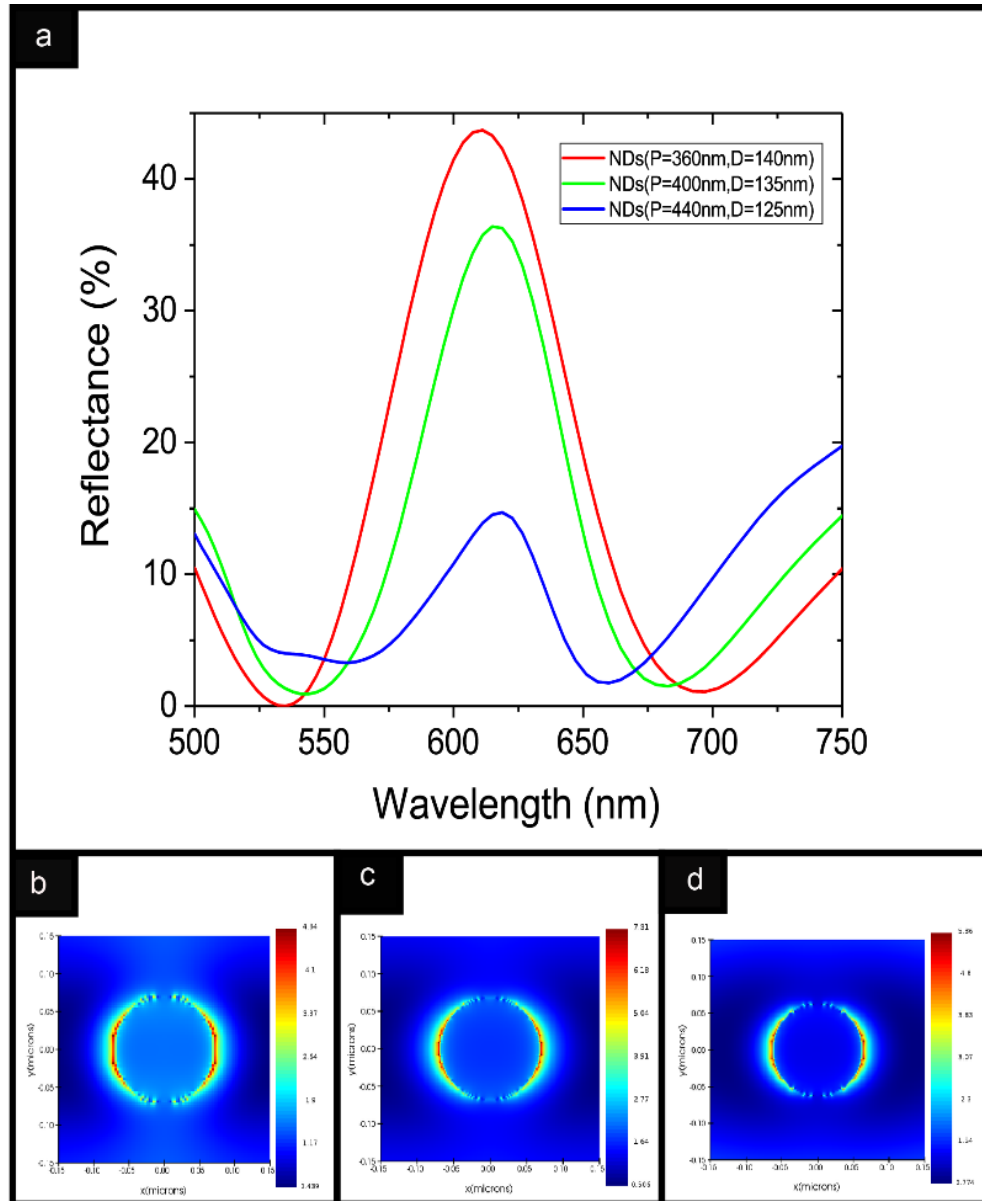
Figure 28. *a) Calculated reflection results of the NDs. b), c) and d) show the corresponded simulated electric field of NDs at resonance wavelength of 604 nm, 610 nm and 595 nm respectively.*

As the reflection band overlaps more efficiently with the emission spectrum of the gain material, the more PL enhancement is expected. Our investigations show that the absorption and reflection bands of NDs have almost the same spectral peak position. Because of non-transparency of the used substrate, instead of the absorption band, the overlap between the reflection and emission spectra are considered. The NDs in which their reflection band overlaps not so effectively with the emission spectrum of the gain material results in less PL enhancement factor. Even though the number of the acceptors (NDs) in target measuring area is highest for 360 nm period sample, less PL enhancement is observed because of the low absorptivity of NDs with the higher diameters. For the period of 440 nm, in the target measuring area the smallest number of acceptors

exist as compared to 360 nm and 400 nm sample. But since the NDs with lower diameters show higher absorption, consequently, the combination of these two effects causes that the NDs with the diameter of 125 nm to present the highest emission enhancement of gain material. However, for 400 nm period sample with higher air gaps between NDs as compared to 360 nm one, the overall measured PL enhancement is higher. As we mentioned before, this happens as a result of a better spectral overlap for NDs with diameter of 135 nm in 400 nm sample with respect to the other arrays. Therefore, much stronger interaction between NDs and dye molecule occurs in this period, resulting in 7 folds of the measured emission enhancement.
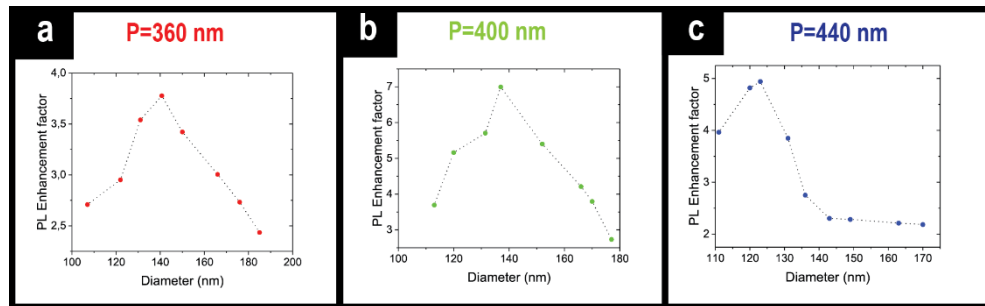
Figure 29. *An enhancement factor of dye molecules emission in the presence of NDs with a) diameter (110-185 nm) and periodicity (360 nm) b) diameter (110-180 nm) and periodicity (400 nm), c) diameter (110-170 nm) and periodicity (440 nm), compared to the emission of dye in the absence of NDs.*

Figure 29 presents the enhancement of factor change based on the diameter change in three different periods. The entire plot shows a trend that the enhancement factor increases with diameter, and after an efficient overlap (between NDs plasmon band and emission band of dye) it decreases again. This figure presents the overlap phenomena of NDs absorption and the emission of LDS750. From Figure 26, how overlap between NDs plasmon resonance and the emission of LDS750 trend is following with diameter. The resulting trend is seen in Figure 29 for PL enhancement factor of dye molecules.

From Figure 26, it is evident that for 360 nm period sample, the NDs with 140 nm diameter have the best spectral overlap with the emission of LDS750 with respect to other NDs with different diameters, resulting in a much more efficient non-radiative energy transfer between donor and acceptor pairs. The overlap between NDs plasmon band and emission band of dye drive the non-radiative energy transfer, which depends on how strong overlap is between these two bands. The same observation is noticeable for 400 nm period sample with 135 nm diameter, as well as, for 440 nm period sample with 125 nm diameter. However, since the absorption of NDs depends on their diameter, the PL enhancement factor is different for the aforementioned NDs with three different periods. From simulation results, 1600, 1680, 1640 times Purcell factor are achieved for the best

sample of 360 nm, 400 nm and 440 nm period, respectively. However, in the experimental results, the acquired enhancement factors are 3.8, 7 and 5 folds for those samples. In the simulation, the orientation of dye molecules dipole moments is considered in all possible directions, and the dipole is placed in different positions of local field and in the end, the calculated Purcell factors are averaged. While in practice, most of the dye molecules are not located in the hot spots of the NDs and consequently, they do not couple efficiently with NDs. As the orientation of emitter dipoles, homogeneous distribution of dye molecules, inter-distance between dye-ND pairs, the air gap between NDs and the smoothness of the fabricated NDs surface are not exactly the same, these imperfections result in degradation of the experimentally acquired Purcell factor.
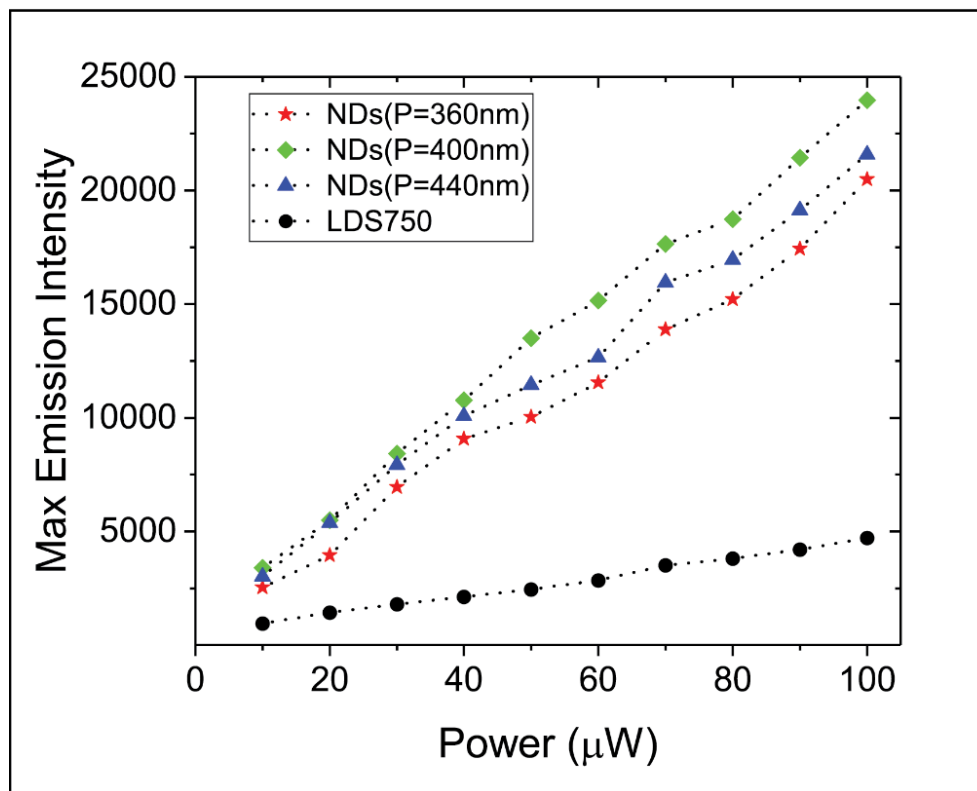
Figure 30. *The power dependence of the emission intensity of LDS750 dye with NDs and without NDs for diameter 140 nm and period 360 nm (red), diameter 135 nm and period 400 nm (green), diameter 125 nm and period 440 nm (blue). Black dot line is the emission intensity of dye in the absence of the dye molecules.*

Figure 30 demonstrates the power dependence of the dye emission in the presence and absence of NDs for maximum PL enhancement observed samples. A CW laser (532nm) is used and a long-pass filter of 600 nm in the path of detection to block exciting wavelength. Power of the laser is changed around 10 uW every time. When the intensity is higher, more dye molecules are excited and more energy transfer non-radiatively to NDs from dye molecules. The local field of NDs is enhanced because of the transferred energy from excited dye molecules to NDs. Enhancement of the local field excites more dye molecules, which leads to metal enhanced fluorescence. This cause the emission

enhancement of dye and increases with the increase of power. More excited dye molecules are enhancing the local field of the NDs, so radiative decay rate also increases, which induced by the local field of NDs. More evidence of energy transfer is performed by lifetime experiment and FLIM, which are based on the lifetime change because of coupling between NDs and excited molecules.

4.6 Time-integrated fluorescence and FLIM of hybrid NDs

In PL enhancement measurements, the collection efficiency of the used system can affect the acquired results, and it can be a considered as one of the reasons for the difference between the simulated and experimental Purcell factor. However, by acquiring the modification of the emission enhancement rate through fluorescence lifetime measurements, the effect of this factor can be neglected. As a result of the resonance coupling between plasmonic NDs and dipoles of excited dye molecules, the decay time of the emitter can be quenched. According to the equation of 2.5.11, the lifetime of the emitter would be shortened, through the non-radiative energy transfer term (k_{ET}) to the plasmonic quencher. Stronger coupling between the emitter and accepter pairs will have resulted in a pronounced shortening of the emitter lifetime. In addition, as it is stated in the equation of 2.5.11, in the presence of plasmonic structure, a new radiative decay channel (Γ_m) is introduced, in which increases the quantum yield of dye molecules and slightly decreases the lifetime. As a consequence, the quantum yield of the emitter can be decreased or increased according to the strength of the enhancing factor introduced by the radiative or non-radiative terms.
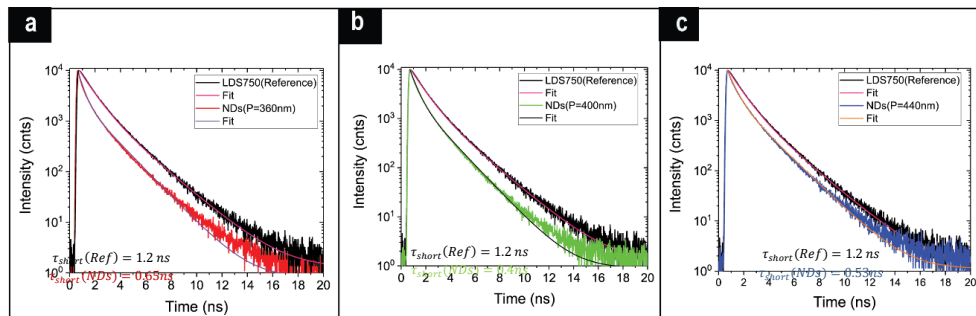
Figure 31.   *Lifetime measurement of reference (LDS750) and LDS750 in the presence of NDs. In a), b), c) shows the shortening of LDS750 lifetime in the presence of NDs for 360 nm, 400 nm, 440 nm period and diameter 140, 135, 125 nm respectively.*

Lifetime plots in Figure 31 validate the shortening of the lifetime in the presence of NDs. The decay rates of the LDS750 are measured in the absence and presence of NDs. This measurement is done by PicoQuant (Hydraharp 400) system, whereas plasmonic hybrid antennas are excited with a pulse laser with a 5 MHz repetition rate at 532 nm at a single

spot. A 535 nm dichroic mirror and a long-pass filter of 600 nm are placed in detection path of a single-photon avalanche diode (MPD). The double exponential fit is used as the best fit function for the acquired decay rate results, in both cases of the absence and presence of NDs. The shortening of lifetime occurs while we excite the plasmonic system through the non-radiative energy transfer between the excited dye molecules and plasmonic acceptors. However, based on the PL enhancement results, the boosting of the radiative channel is another reason for the shortening of the lifetime. In the investigation of the emission of dye molecules, we perceived the increase of the PL intensity as 3.8, 7 and 5 folds for 360 nm, 400 nm and 440 nm periods, respectively. However, the lifetime decrease is in between 2 to 2.5 times for each one of these NDs arrays. The lifetime of dye depends on radiative and non-radiative decay rates, but the emission enhancement factor depends on other parameters such as the local field intensity of NDs, lightning rod effect, dipole orientation and position of dye molecules in the excited spot [109]. Therefore, the rate of lifetime change is different than the reported emission enhancement factor. In addition, for higher emission enhancement factor, more shortening of lifetimes are expected. This fact is validated by comparing the trend of the lifetime change, and PL enhancement change of the coupled dye molecules to plasmonic NDs. For the mentioned specific diameter of each NDs array, the dye molecules have the highest coupling efficiency, which leads to the highest shortening of donor lifetime. Figure 31 indicates the lifetime of LDS750 as 1.2 ns in uncoupled case, while it changes to 0.65, 0.4 and 0.53 ns when is coupled to plasmon modes of NDs with diameter of 140 nm (360 nm period), 135 nm (400 nm period) and 125 nm (440 nm period), respectively.

FLIM experiments also are performed to indicate the lifetime modification of dye molecules in a specific area of the excited sample. FLIM images are the visual representation of the lifetime components of the donor in the presence and absence of acceptor. In Figure 32, (c, d) the fast and slow components of the LDS750 lifetime placed on top of NDs with (c, d) diameter of 140 nm (360 nm period), (e, f) diameter of 135 nm (400 nm period) and (g, h) diameter of 125 nm (440 nm period) are presented. In FLIM, different pixels of the hybrid plasmonic system is scanned to acquire the modification of lifetime of the LDS750 dye molecules in the presence and absence of NDs. FLIM images are made based on the lifetime of LDS750 for each pixel of the scanned area. Thus, a complete image reflects the contrast between the different decay rates of each pixel in the scanned area as a colour change. The average lifetime of the excited dye is calculated for the scanned area. This experiment is performed by using a pulse laser (532 nm) with 20 MHz repetition rate in 200×200 pixels of the area and 600 nm long-pass filter is used in the detection path to block the excitation beam towards the APD detector.
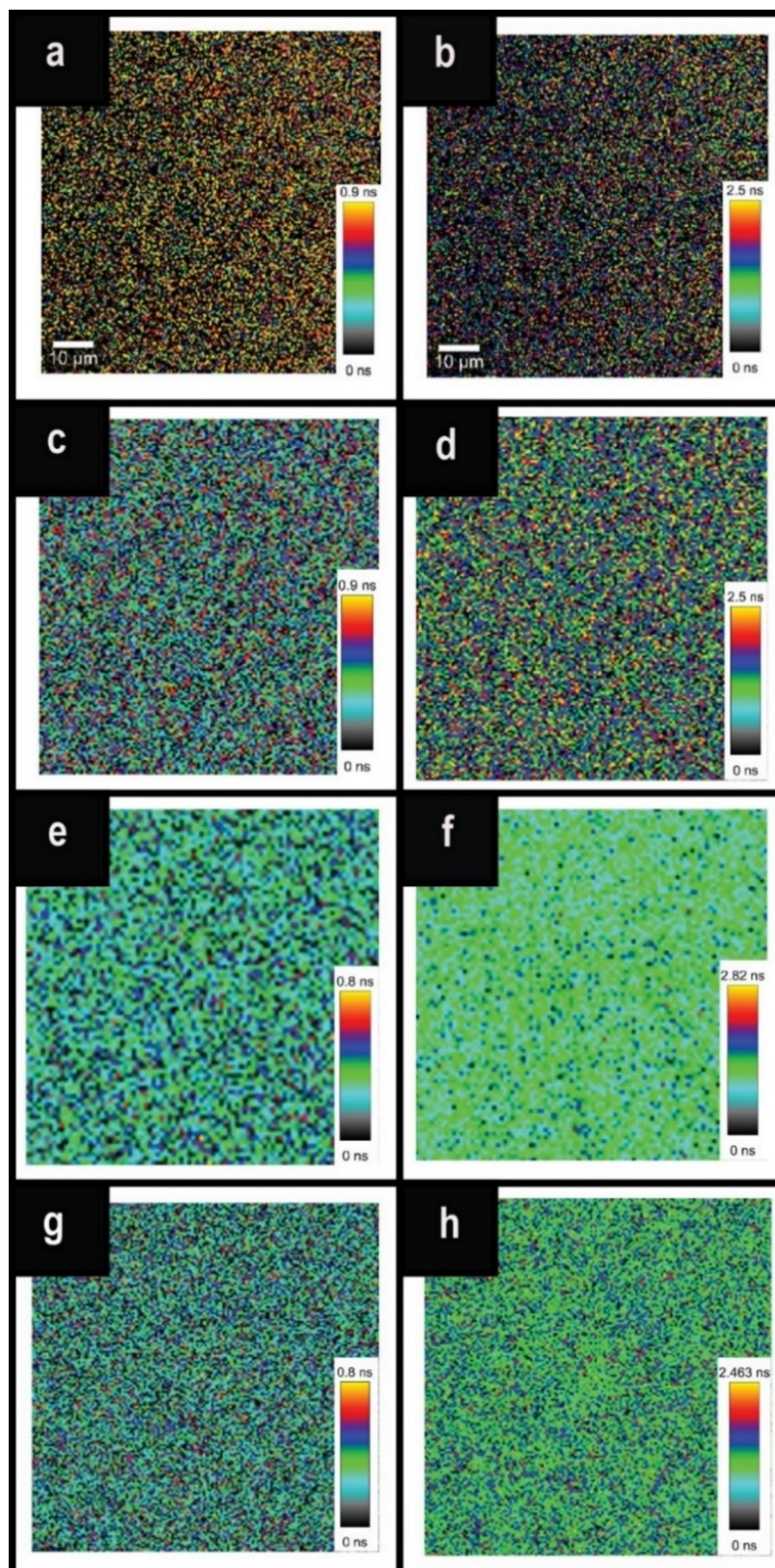
Figure 32. *FLIM image of lifetime change of LDS750 in the absence and presence of NDs. Figure a), b) represents the fast and slow lifetime components of dye in the absence of NDs. Figure c), e), g) is the fast lifetime component of the best overlap NDs sample for 360, 400, 440 nm period, while d), f), h) represents the slow lifetime component of those samples respectively.*

Colour bar represents the lifetime range of LDS750, so a change in colour of the FLIM image denotes the change of the lifetime component of LDS750 for each of the pixels. As the distribution and orientation of dye molecules are different in each pixel, so colour contrast from one pixel to another one is observed. The colour contrast is related to the different coupling rate for different periods and diameters, so FLIM images are expected to appear differently. The brighter pixels in FLIM images can be attributed to the lifetime of dye molecules in the absence of NDs. In fact, the darker spots are related to the fast component of a lifetime, resulted from the stronger coupling. The colour contrast in lifetime of dye molecules in the presence and absence of NDs is evident, because of the occurred coupling between the excited dye dipole and NDs. The fast component is indicating a strong coupling with NDs. The slow component has less contribution to lifetime shortening. Therefore, only the fast component of lifetime is considered in interpretation of results. Extracted histogram from the FLIM images represents different lifetime components of dye molecules based on the coupling rate. As it shows in Figure 33a has a fast component in the time range of 0.9 ns. Now, comparing the lifetime of the dye molecules in the presence of NDs in a period of 360 nm, 400 nm and 440 nm, we have the fast component values as 0.5, 0.28 and 0.36 ns (Figure 33 c, e, g), respectively. These values are in agreement with the emission enhancement results, as we have seen more emission enhancement in 400 nm period with 7 folds. The slow component of lifetime stays almost the same for all these samples. The observed difference between extracted lifetime components based on the decay curves and FLIM histograms is related to the difference in collection spots in each one of these experiments.
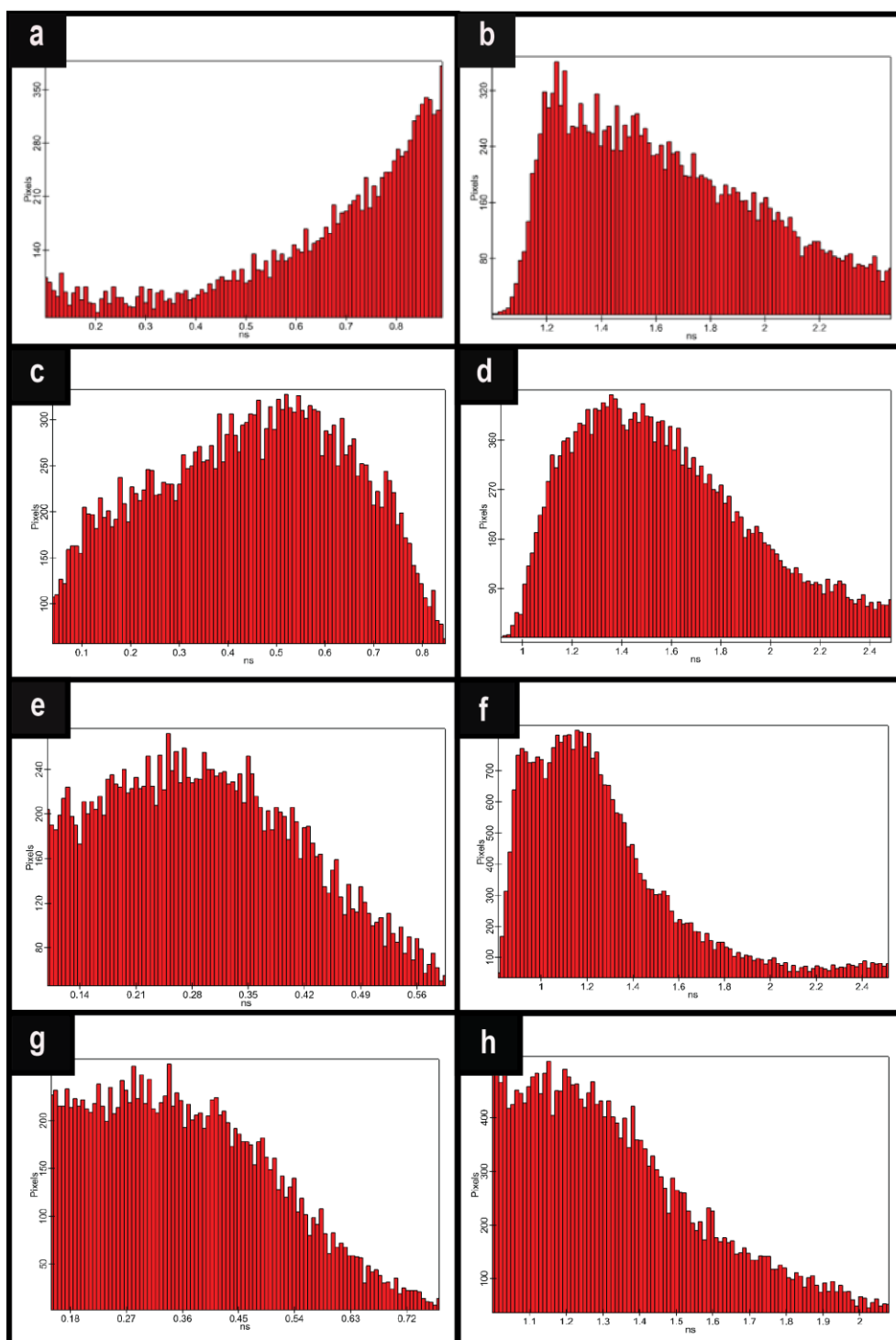
Figure 33. *Histogram of the dye's lifetime component in the absence (a, b), and presence of the NDs for 360 nm (c, d), 400 nm (e, f), 440 nm (g, h) period sample. Figure (a, c, e, g) are the fast and (b, d, f, h) are the slow component.*

5. CONCLUSIONS AND FUTURE WORK

In this thesis, we demonstrated metal enhanced fluorescence using NDs array. We investigated the plasmonic resonance wavelength by changing the size and period of the NDs array. Effect of the substrate and ND size on fluorescence enhancement is observed by using LDS750 dye which has a suitable spectrum.

First of all, the glass substrate is not suitable for this study because the required adhesion layer (Cr, Ti) inhibits the plasmon resonance. In addition, because glass has a higher refractive index than Si-SiO$_2$ substrate and this shifts the resonance band of NDs array to higher wavelengths 40-50 nm. Dependence of plasmon resonance on the dielectric environment also investigated. The dielectric environment plays a vital role in plasmon resonance. When PMMA used as the dielectric environment, the resonance band shifts to higher wavelengths. Therefore, the resonance band of NDs should be considered with PMMA because PMMA is the host medium of dye. Moreover, the thickness of the PMMA layer as low as possible is needed for better coupling. Thinner PMMA layer decreases the overall distance between NDs and LDS750 dye molecules. On the other hand, a spacer layer between NDs and dye is essential to reduce quenching probability because of direct contact of emitters to the metal.

By changing the diameter or period of NDs, the spectral overlap of the NDs plasmon resonance spectrum and emission band of LDS750 is modified to achieve higher Purcell factor enhancement. In this work, 2-7-fold of spontaneous emission rate enhancement is obtained by changing the diameter and period of NDs. To achieve the best coupling with the electric dipole of emitters, the diameter of NDs is varied from 105-195 nm while 3 different periods (360 nm, 400 nm and 440 nm) is used. It is observed that for the optimum coupling, both diameter and period are effective. Higher quality factor plasmon resonance is obtained with a lower period and diameter which increases the Purcell factor enhancement. Overall, the antenna dipole resonance (plasmonic resonance) should couple to the emitter's electric dipole moment for the best enhancement factors. However, the random orientation of emitters and the quality of the fabricated NDs decrease the Purcell factor enhancement.

Moreover, the emission enhancement of the dye molecules depends on the power of incident light. It may increase the interaction between the local field of NDs and LDS750 dye molecules by exciting more emitters. FLIM and lifetime experiment results present

the coupling between the local field of NDs and dye molecules. However, emission enhancement of LDS750 is observed 2-7 times while lifetime changes ware 2-3 times. This is due to the power difference of the incidence of light, lightning rod effect, and data collection from the different environment in these two measurements. As we excite the different part of the NDs array with different excitation power, it may change the number of excited dye molecules. Also, different parts of the NDs are covered with different orientation of the dye molecules and have different overall coupling. With same power and incident spot in the NDs, we would have achieved similar results from both experiments. Lifetime difference between FLIM and decay curve is observed because decay data are collected from the single spot while FLIM results are the average lifetime of the scanned area. But except this all the results are in agreement with the emission enhancement of LDS750 for all the NDs samples.

From the application point of view, our designed NDs can be applied for light boosting. They can be exploited as a light-emitting device with the right combination of nanoantennas and emitters by increasing the quantum efficiency of emitters. In this work, the metallic loss can be minimized with some nanofabrication techniques. By applying the appropriate condition to our hybrid system, it can be used in lasing purpose. In addition, this work can be extended to investigate the light-matter interaction by using QDs, h-BN (hexagonal boron nitride) layers with NDs.

I have also numerically investigated a new nanostructure in an ellipse shape, which can provide two plasmon resonance (Figure 34). These nano-ellipses (NEs) can be used as polarization-dependent or independently based on their unit cell design. TSPR (transversal surface plasmon resonance) and LSPR (longitudinal surface plasmon resonance) of NEs can be used to enhance the excitation rate as well as the emission rate. Moreover, two resonances can be useful to enhance the emission of two dyes in the same solution, simultaneously. In the case of polarization-dependent NEs design, it can be used by either its TSPR or LSPR. These light-matter interaction properties for NEs by using emitters will be investigated in future work.

6. REFERENCE

[1] Razzari L, Toma A, Clerici M, Shalaby M, Das G, Liberale C, et al. Terahertz Dipole Nanoantenna Arrays: Resonance Characteristics. Plasmonics. 2013;8(1):133–8.

[2] Ozbay E. Plasmonics : Merging Photonics and Electronics at Nanoscale Dimensions. Science (80-). 2006;311(2006):189–94.

[3] Kress BC. Subwavelength Optics. F Guid to Digit Micro-Optics. 2015;424(August):824–30.

[4] Muskens OL, Giannini V, Sánchez-Gil JA, Gómez Rivas J. Strong enhancement of the radiative decay rate of emitters by single plasmonic nanoantennas. Nano Lett. 2007;7(9):2871–5.

[5] Ko H, Singamaneni S, Tsukruk V V. Nanostructured surfaces and assemblies as SERS media. Small. 2008. 1576–99.

[6] Brown RJC, Milton MJT. Nanostructures and nanostructured substrates for surface-enhanced Raman scattering (SERS). Journal of Raman Spectroscopy. 2008. 1313–26.

[7] Hyyti J, Perestjuk M, Mahler F, Grunwald R, Güell F, Gray C, et al. Field enhancement of multiphoton induced luminescence processes in ZnO nanorods. J Phys D Appl Phys. 2018 Feb 19;51(10).

[8] Mahmoud MA, Tabor CE, El-Sayed MA. Surface-enhanced raman scattering enhancement by aggregated silver nanocube monolayers assembled by the Langmuir-Blodgett technique at different surface pressures. J Phys Chem C. 2009 Apr 9;113(14):5493–501.

[9] Kelly KL, Coronado E, Zhao LL, Schatz GC. The optical properties of metal nanoparticles: The influence of size, shape, and dielectric environment. J Phys Chem B. 2003;107(3):668–77.

[10] Sihvola A. Dielectric Polarization and Particle Shape Effects. J Nanomater. 2007:1–9.

[11] Khlebtsov BN, Khlebtsov NG. Multipole plasmons in metal nanorods: Scaling properties and dependence on particle size, shape, orientation, and dielectric environment. J Phys Chem C. 2007 Aug 9;111(31):11516–27.

[12] Zhao Y, Engheta N, Alù A. Effects of shape and loading of optical nanoantennas on their sensitivity and radiation properties. J Opt Soc Am B. 2011 May 1;28(5):1266.

[13] Jain PK, Huang X, El-Sayed IH, El-Sayed MA. Noble metals on the nanoscale: Optical and photothermal properties and some applications in imaging, sensing, biology, and medicine. Acc Chem Res. 2008 Dec 16;41(12):1578–86.

[14] El-Sayed MA. Some interesting properties of metals confined in time and nanometer space of different shapes. Acc Chem Res. 2001;34(4):257–64.

[15] Link S, Mohamed MB, El-Sayed MA. Simulation of the Optical Absorption Spectra of Gold Nanorods as a Function of Their Aspect Ratio and the Effect of the Medium Dielectric Constant. J Phys Chem B. 1999 Apr;103(16):3073–7. Available from: https://pubs.acs.org/doi/10.1021/jp990183f

[16] Knight MW, Liu L, Wang Y, Brown L, Mukherjee S, King NS, et al. Aluminum plasmonic nanoantennas. Nano Lett. 2012 Nov 14;12(11):6000–4.

[17] Cubukcu E, Kort EA, Crozier KB, Capasso F. Plasmonic laser antenna. Appl Phys Lett. 2006;89(9).

[18] Smythe EJ, Cubukcu E, Capasso F. Optical properties of surface plasmon resonances of coupled metallic nanorods. Opt Express. 2007;15(12):7439.

[19] Wang Q, Liu L, Wang Y, Liu P, Jiang H, Xu Z, et al. Tunable Optical Nanoantennas Incorporating Bowtie Nanoantenna Arrays with Stimuli-Responsive Polymer. Sci Rep. 2015 Dec 18;5.

[20] Costa KQ da, Dmitriev VA. Analysis of modified bowtie nanoantennas in the excitation and emission regimes. J Microwaves, Optoelectron Electromagn Appl. 2011 Jun;10(1):232–42. Available from: http://www.scielo.br/scielo.php?script=sci_arttext&pid=S2179-10742011000100021&lng=en&tlng=en

[21] Kaniber M, Schraml K, Regler A, Bartl J, Glashagen G, Flassig F, et al. Surface plasmon resonance spectroscopy of single bowtie nano-antennas using a differential reflectivity method. Sci Rep. 2016 Mar 23;6.

[22] Shu F-Z, Zhang L-H, Wang J-N, Peng R-W, Fan R-H, Qi D-X, et al. Dynamically tunable bowtie nanoantennas based on the phase transition of vanadium dioxide. Opt Lett. 2019 Jun 1;44(11):2752.

[23] Feng L, Ma R, Wang Y, Xu D, Xiao D, Liu L, et al. Silver-coated elevated bowtie nanoantenna arrays: Improving the near-field enhancement of gap cavities for highly active surface-enhanced Raman scattering. Nano Res. 2015 Sep 25;8(11):3715–24.

[24] Chou Chau YF, Chou Chao CT, Rao JY, Chiang HP, Lim CM, Lim RC, et al. Tunable Optical Performances on a Periodic Array of Plasmonic Bowtie Nanoantennas with Hollow Cavities. Nanoscale Res Lett. 2016 Dec 1;11(1).

[25] Uemoto M, Ajiki H. Conditions for stronger field enhancement of semiconductor bowtie nanoantennas. Opt Lett. 2015 Apr 15;40(8):1695.

[26] Melchior P, Bayer D, Schneider C, Fischer A, Rohmer M, Pfeiffer W, et al. Optical near-field interference in the excitation of a bowtie nanoantenna. Phys Rev B - Condens Matter Mater Phys. 2011 Jun 8;83(23).

[27] Wu E, Chi Y, Wu B, Xia K, Yokota Y, Ueno K, et al. Spatial polarization sensitivity of single Au bowtie nanostructures. J Lumin. 2011 Sep;131(9):1971–4.

[28] Gómez-Medina R, Yamamoto N, Nakano M, De Abajo FJG. Mapping plasmons in nanoantennas via cathodoluminescence. New J Phys. 2008 Oct 28;10.

[29] Ming T, Zhao L, Yang Z, Chen H, Sun L, Wang J, et al. Strong polarization dependence of plasmon-enhanced fluorescence on single gold nanorods. Nano Lett. 2009 Dec 11;9(11):3896–903.

[30] Ming T, Zhao L, Chen H, Woo K, Wang J, letters HL-N, et al. Experimental evidence of plasmophores: plasmon-directed polarized emission from gold nanorod–fluorophore hybrid nanostructures. ACS Publ. Available from: https://pubs.acs.org/doi/abs/10.1021/nl200535y

[31] Chen H, Shao L, Li Q, Reviews JW-CS. Gold nanorods and their plasmonic properties. pubs.rsc.org. Available from: https://pubs.rsc.org/en/content/articlehtml/2013/cs/c2cs35367a

[32] Kern J, Trügler A, Niehues I, JE-A. Nanoantenna-Enhanced Light–Matter Interaction in Atomically Thin WS2. ACS Publ. Available from: https://pubs.acs.org/doi/abs/10.1021/acsphotonics.5b00123

[33] Schniepp H, Sandoghdar V. Spontaneous emission of europium ions embedded in dielectric nanospheres. Phys Rev Lett. 2002;89(25):257403/1-257403/4.

[34] Rogobete L, Kaminski F, Agio M, Sandoghdar V. Design of plasmonic nanoantennae for enhancing spontaneous emission. Opt Lett. 2007;32(12):1623.

[35] Viste P, Plain J, Jaffiol R, Vial A, Adam PM, Royer P. Enhancement and Quenching Regimes in Metal−Semiconductor Hybrid Optical Nanosources. ACS Nano. 2010 Feb 23;4(2):759–64. Available from: http://pubs.acs.org/doi/10.1021/nn901294d

[36] Kulakovich O, Strekal N, Yaroshevich A, Maskevich S, Gaponenko S, Nabiev I, et al. Enhanced Luminescence of CdSe Quantum Dots on Gold Colloids. 2002; Available from: https://pubs.acs.org/doi/abs/10.1021/nl025819k

[37] Liu S-Y, Huang L, Li J-F, Wang C, Li Q, Xu H-X, et al. Simultaneous Excitation and Emission Enhancement of Fluorescence Assisted by Double Plasmon

Modes of Gold Nanorods. J Phys Chem C. 2013 May 23.117(20):10636–42. Available from: http://pubs.acs.org/doi/10.1021/jp4001626

[38] Wang H. Plasmonic refractive index sensing using strongly coupled metal nanoantennas: Nonlocal limitations. Sci Rep. 2018 Dec 1;8(1).

[39] Rusak E, Staude I, Decker M, Sautter J, Miroshnichenko AE, Powell DA, et al. Hybrid nanoantennas for directional emission enhancement. Appl Phys Lett. 2014 Dec 1;105(22).

[40] Taminiau TH, Stefani FD, van Hulst NF. Enhanced directional excitation and emission of single emitters by a nano-optical Yagi-Uda antenna. Opt Express. 2008 Jul 7;16(14):10858. Available from: https://www.osapublishing.org/abstract.cfm?URI=oe-16-14-10858

[41] Mahmoud MA, Chamanzar M, Adibi A, El-Sayed MA. Effect of the dielectric constant of the surrounding medium and the substrate on the surface plasmon resonance spectrum and sensitivity factors of highly symmetric systems: Silver nanocubes. J Am Chem Soc. 2012 Apr 11;134(14):6434–42.

[42] Forcherio GT, Blake P, Seeram M, DeJarnette D, Roper DK. Coupled dipole plasmonics of nanoantennas in discontinuous, complex dielectric environments. J Quant Spectrosc Radiat Transf. 2015 Nov 1;166:93–101.

[43] Toudert J, Simonot L, Camelio S, Babonneau D. Advanced optical effective medium modeling for a single layer of polydisperse ellipsoidal nanoparticles embedded in a homogeneous dielectric medium: Surface plasmon resonances. Phys Rev B - Condens Matter Mater Phys. 2012 Jul 10;86(4).

[44] Jain PK, Huang X, El-Sayed IH, El-Sayed MA. Review of some interesting surface plasmon resonance-enhanced properties of noble metal nanoparticles and their applications to biosystems. Plasmonics. 2007 Sep;2(3):107–18.

[45] Underwood S, Mulvaney P. Effect of the Solution Refractive Index on the Color of Gold Colloids. Langmuir. 1994 Oct 1;10(10):3427–30.

[46] Jensen TR, Duval ML, Kelly KL, Lazarides AA, Schatz GC, Van Duyne RP. Nanosphere Lithography: Effect of the External Dielectric Medium on the Surface Plasmon Resonance Spectrum of a Periodic Array of Silver Nanoparticles. J Phys Chem B. 1999 Nov;103(45):9846–53. Available from: https://pubs.acs.org/doi/10.1021/jp9926802

[47] Kadkhodazadeh S, Christensen T, Beleggia M, Mortensen NA, Wagner JB. The Substrate Effect in Electron Energy-Loss Spectroscopy of Localized Surface Plasmons in Gold and Silver Nanoparticles. ACS Photonics. 2017 Feb 15;4(2):251–61.

[48]   Ghosh SK, Nath S, Kundu S, Esumi K, Pal T. Solvent and ligand effects on the localized surface plasmon resonance (LSPR) of gold colloids. J Phys Chem B. 2004 Sep 16;108(37):13963–71.

[49]   Xu G, Tazawa M, Jin P, Nakao S, Yoshimura K. Wavelength tuning of surface plasmon resonance using dielectric layers on silver island films. Appl Phys Lett. 2003 Jun 2;82(22):3811–3.

[50]   Duval Malinsky M, Kelly KL, Schatz GC, Van Duyne RP. Nanosphere Lithography: Effect of Substrate on the Localized Surface Plasmon Resonance Spectrum of Silver Nanoparticles. J Phys Chem B. 2001 Mar;105(12):2343–50. Available from: https://pubs.acs.org/doi/10.1021/jp002906x

[51]   Valamanesh M, Borensztein Y, Langlois C, Lacaze E. Substrate effect on the plasmon resonance of supported flat silver nanoparticles. J Phys Chem C. 2011 Feb 24;115(7):2914–22.

[52]   Knight MW, Wu Y, Lassiter JB, Nordlander P, Halas NJ. Substrates matter: influence of an adjacent dielectric on an individual plasmonic nanoparticle. Nano Lett. 2009 May 13;9(5):2188–92.

[53]   Martinsson E, Otte MA, Shahjamali MM, Sepulveda B, Aili D. Substrate effect on the refractive index sensitivity of silver nanoparticles. J Phys Chem C. 2014 Oct 23;118(42):24680–7.

[54]   Sikdar D, Zhu W, Cheng W, Premaratne M. Substrate-Mediated Broadband Tunability in Plasmonic Resonances of Metal Nanoantennas on Finite High-Permittivity Dielectric Substrate. Plasmonics. 2015 Dec 1;10(6):1663–73.

[55]   Novotny L, Hecht B. Principles of Nano-Optics. New York, NY: Cambridge University Press; 1385. 302.

[56]   Maier SA. Plasmonics:Fundamentals and Applications. Physics. 2004. 10. Available from: http://elib.tu-darmstadt.de/tocs/95069577.pdf

[57]   Maier SA. Plasmonics : Fundamentals and applications. 2007.

[58]   Shahbazyan T V, Stockman MI. Plasmonics : Theory and applications. Springer+Business Media Dordrecht;

[59]   Zayats A V., Smolyaninov II, Maradudin AA. Nano-optics of surface plasmon polaritons. Phys Rep. 2005 Mar 1;408(3–4):131–314. Available from: https://www.sciencedirect.com/science/article/pii/S0370157304004600?via%3Dihub

[60]   Smith CLC, Stenger N, Kristensen A, Mortensen NA, Bozhevolnyi SI. Gap and channeled plasmons in tapered grooves: a review. Nanoscale. 2015 May 21;7(21):9355–86. Available from: http://xlink.rsc.org/?DOI=C5NR01282A

[61] Willets KA, Van Duyne RP. Localized Surface Plasmon Resonance Spectroscopy and Sensing. Annu Rev Phys Chem. 2007 May;58(1):267–97.

[62] Hewageegana P, Stockman MI. Plasmonic enhancing nanoantennas for photodetection. Infrared Phys Technol. 2007 Apr;50(2–3):177–81.

[63] Giannini V, Fernández-Domínguez AI, Heck SC, Maier SA. Plasmonic Nanoantennas: Fundamentals and Their Use in Controlling the Radiative Properties of Nanoemitters. Chem Rev. 2011;111(6):3888–912.

[64] Jeanmonod DJ, Rebecca, Suzuki K et al., Hrabovsky M, Mariana Furio Franco Bernardes MP, Lilian Cristina Pereira and Daniel Junqueira Dorta. Enhanced molecular specroscopy via localized surface plasmon resonance. Intech open. 2018;2:64.

[65] Barnes WL. Particle plasmons: Why shape matters. 2016;(3):1–10. Available from: http://arxiv.org/abs/1609.04184%0Ahttp://dx.doi.org/10.1119/1.4948402

[66] Kausar ASMZ, Reza AW, Latef TA, Ullah MH, Karim ME. Optical nano antennas: State of the art, scope and challenges as a biosensor along with human exposure to nano-toxicology. Sensors (Switzerland). 2015;15(4):8787–831.

[67] F. Bohren C, R.Huffman D. Absorotion and Scattering of light by small particles. Wiley; 1983.

[68] Evanoff DD, Chumanov G. Size-controlled synthesis of nanoparticles. 2. Measurement of extinction, scattering, and absorption cross sections. J Phys Chem B. 2004;108(37):13957–62.

[69] Moroz A. Depolarization field of spheroidal particles. 2009;26(3):517–27.

[70] Faulkner LR. Absorption of light and ultraviolet radiation: fluorescence and phosphorescence emission (Schenk, George H.). J Chem Educ. 1974 Sep 1;51(9):A454. Available from: https://doi.org/10.1021/ed051pA454.2

[71] Link S, El-sayed MA. International Reviews in Physical Chemistry Shape and size dependence of radiative, non-radiative and photothermal properties of gold nanocrystals. Intern Rev Phys Chem. 2000;19(3):409–53.

[72] Lee JW. Bioluminescence. 2017;(January).

[73] Lakowicz JR. Principles of Fluorescence Spectroscopy. Principles of fluorescence spectroscopy, Springer, New York, USA, 3rd edn, 2006. 362.

[74] Udayan S, Sha M M R, Sebastian M, Nampoori VPN, Thomas S. Two photon induced amplified spontaneous emission at low threshold from Styryl 7 dye incorporated DNA template. Opt Mater (Amst). 2018;86(September):492–7. Available from: https://doi.org/10.1016/j.optmat.2018.10.046

[75] Goldys EM. Applications in Biotechnology and the life sciences. New Jersy: Wiley-Blackwell; 2009.

[76] Wild D. The Immunoassay Handbook. Fourth. Elsevier; 2013.

[77] Biagioni P. Nanoantennas for visible and infrared radiation. 2012;(February).

[78] Zhang Y, Clapp A. Overview of stabilizing ligands for biocompatible quantum dot nanocrystals. Sensors. 2011;11(12):11036–55.

[79] Michalet X, Pinaud FF, Bentolila LA, Tsay JM, Doose S, Li JJ, et al. Quantum dots for live cells, in vivo imaging, and diagnostics. Science. 2005 Jan 28;307(5709):538–44. Available from: https://www.ncbi.nlm.nih.gov/pubmed/15681376

[80] Geddes C. Metal-enhanced fluorescence. 2010; Available from: https://www.google.com/books?hl=fi&lr=&id=akgpFdT9sA8C&oi=fnd&pg=PR5&dq=metal+enhanced+fluorescence&ots=xEnZGoIe5T&sig=XyUMRXSohT9LdJXxlSQ_o4RXdg0

[81] Kabbash M El, Rashed AR, Sreekanth KV, De Luca A, Infusino M, Strangi G. Plasmon-Exciton Resonant Energy Transfer: Across Scales Hybrid Systems. 2016; Available from: http://dx.doi.org/10.1155/2016/4819040

[82] Gurlek B, Sandoghdar V. Manipulation of quenching in nanoantenna-emitter systems enabled by external detuned cavities : a path to enhance. :1–18.

[83] Gan W, Tserkezis C, Cai Q, Falin A, Mateti S, Nguyen M, et al. Atomically Thin Boron Nitride as an Ideal Spacer for Metal-Enhanced Fluorescence. ACS Nano. 2019 Oct 7;

[84] Liu M, Lee TW, Gray SK, Guyot-Sionnest P, Pelton M. Excitation of dark plasmons in metal nanoparticles by a localized emitter. Phys Rev Lett. 2009 Mar 9;102(10).

[85] Krasnok AE, Slobozhanyuk AP, Simovski CR, Tretyakov SA, Poddubny AN, Miroshnichenko AE, et al. An antenna model for the Purcell effect. Sci Rep. 2015;5:1–16.

[86] Krasnok AE, Slobozhanyuk AP, Simovski CR, Tretyakov SA, Poddubny AN, Miroshnichenko AE, et al. An antenna model for the Purcell effect. Sci Rep. 2015;5:1–16. Available from: http://dx.doi.org/10.1038/srep12956

[87] Sauvan C, Hugonin JP, Maksymov IS, Lalanne P. Theory of the spontaneous optical emission of nanosize photonic and plasmon resonators. Phys Rev Lett. 2013 Jun 5;110(23).

[88] Taflove A. Application of the Finite-Difference Time-Domain Method to Sinusoidal Steady-State Electromagnetic-Penetration Problems. IEEE Trans Electromagn Compat. 1980;EMC-22(3):191–202.

[89] Sani A, Zhao Y, Hao Y, Alomainy A, Parini C. An efficient FDTD algorithm based on the equivalence principle for analyzing onbody antenna performance. IEEE Trans Antennas Propag. 2009;57(4 PART. 1):1006–14.

[90] Yee KS. Yee: Solution of Initial Boundary Value Problems. Ieee Trans Antennas Propag. 1966;AP-14(3):302. Available from: http://citeseerx.ist.psu.edu/viewdoc/download;jsessionid=1F04C91FD6EB0B395 5B15FF839D2AD4D?doi=10.1.1.172.6957&rep=rep1&type=pdf

[91] Ward L. Optical Constants of Eight Rare Earth Elements: (Ce), (Sm), (Gd), (Tb), (Dy), (Er), (Tm), and (Yb) A2 - Palik, Edward D. BT - Handbook of Optical Constants of Solids. 287–340. Available from: https://www.sciencedirect.com/science/article/pii/B9780125444156501059

[92] Johnson PB, Christy RW. Optical constants of the noble metals. Phys Rev B. 1972;6(12):4370–9.

[93] Larson RG, Rehg TJ. Spin Coating. Liq Film Coat. 2011;38(12):709–34.

[94] Xu X, Xia C, Huang S, Peng D. YSZ thin films deposited by spin-coating for IT-SOFCs. Ceram Int. 2005;31(8):1061–4.

[95] Scriven LE. Physics and Applications of DIP Coating and Spin Coating. MRS Proc. 1988 Feb 25;121:717. Available from: https://www.cambridge.org/core/product/identifier/S1946427400485180/type/jour nal_article

[96] Dobrzański LA, Szindler M. Sol gel TiO 2 antireflection coatings for silicon solar cells. 2015;(May 2012).

[97] Yang H, Jin A, Luo Q, Li J, Gu C, Cui Z. Electron beam lithography of HSQ/PMMA bilayer resists for negative tone lift-off process. Microelectron Eng. 2008 May;85(5–6):814–7.

[98] Vieu C, Carcenac F, Pépin A, Chen Y, Mejias M, Lebib A, et al. Electron beam lithography: Resolution limits and applications. Appl Surf Sci. 2000;164(1–4):111–7.

[99] Marrian CRK. Electron-beam lithography with the scanning tunneling microscope. J Vac Sci Technol B Microelectron Nanom Struct. 1992 Nov;10(6):2877.

[100] Ahmadi S, Asim N, Alghoul MA, Hammadi FY, Saeedfar K, Ludin NA, et al. The Role of Physical Techniques on the Preparation of Photoanodes for Dye

Sensitized Solar Cells. Int J Photoenergy. 2014;2014:1–19. Available from: http://www.hindawi.com/journals/ijp/2014/198734/

[101] Takenaka H, Todokoro Y. A PMMA/PMGI Two Layer Resist System for Stable Lift-off Processing. In: Electron-Beam, X-Ray, and Ion-Beam Technology: Submicrometer Lithographies . SPIE; 1989.132.

[102] Chen Y, Peng K, Cui Z. A lift-off process for high resolution patterns using PMMA/LOR resist stack. In: Microelectronic Engineering. Elsevier; 2004. 278–81.

[103] Zhou W, Apkarian RP, Lin Wang Z, Joy D. Fundamentals of Scanning Electron Microscopy.

[104] Zhu FY, Wang QQ, Zhang XS, Hu W, Zhao X, Zhang HX. 3D nanostructure reconstruction based on the SEM imaging principle, and applications. Nanotechnology. 2014 May 9;25(18).

[105] Zhou W, Wang ZL. Scanning Microscopy for Nanotechnology. 2006.

[106] Chauhan A. Deformation and damage mechanisms of ODS steels under high-temperature cyclic loading. Int J Fatigue. 2018;93:1–17. Available from: https://publikationen.bibliothek.kit.edu/1000080339

[107] Becker W. Fluorescence lifetime imaging - techniques and applications. J Microsc. 2012 Aug;247(2):119–36.

[108] Ko CT, Han YY, Chen CH, Shieh J, Chen MJ. Enormous plasmonic enhancement and suppressed quenching of luminescence from nanoscale ZnO films by uniformly dispersed atomic-layer-deposited platinum with optimized spacer thickness. J Phys Chem C. 2013 Dec 12;117(49):26204–12.

[109] Kinkhabwala A, Yu Z, Fan S, Avlasevich Y, Müllen K, Moerner WE. Large single-molecule fluorescence enhancements produced by a bowtie nanoantenna. Nat Photonics. 2009 Nov;3(11):654–7.

7. APPENDIX

<u>Number of dye calculation</u>

Ratio concentration = 0.01% = 0.0001

$$\frac{Mass\ of\ dye\ (QE)}{mass\ of\ solution} = 0.0001$$

$$\rho_{anisole} = 995\ {}^{kg}/_{m^3}$$

$$= 0.995\ {}^{g}/_{mL}\ \text{[PMMA density in solution is neglected]}$$

So, $\rho_{anisole} = \rho_{PMMA\ A4}$

V= volume of the container

Assume,

V= 8 mL,

So, $m_{anisole} = 8\ mL \times 0.995\ {}^{g}/_{mL} = 7.96\ g$ [Possible measurement in gram from balance]

Mass of Dye = 7.96 g × 0.0001

$= 7.96 \times 10\text{-}4\ g$ [it also possible to measure at the beginning of solution preparation by balance in gram unit]

The volume of PMMA around NDs Matrix

V = NDs Matrix area × Thickness of PMMA layer

$= 100\ \mu m \times 100\ \mu m \times 50\ nm$

$= 5 \times 10^{-16}\ m^3$

The mass ratio of PMMA and LDS750 (after evaporation of solvent)

$$\frac{Mass\ of\ dye}{Mass\ of\ PMMA} = \frac{\frac{Mass\ of\ dye}{Mass\ of\ solution}}{\frac{Mass\ of\ PMMA}{Mass\ of\ solution}} = \frac{0.01\%}{4\%} = 0.25\ \%\ \text{[4\% is depends on what percentage}$$

of PMMA and anisole solution is used]

Molar mass of LDS = 484 ${}^{g}/_{mol}$

$$\rho_{PMMA} = \frac{m_{PMMA}}{V_{PMMA}}$$

Density of PMMA = 1.18 $g_{/mL}$

Mass of PMMA = $1.18 \; g_{/mL} \; \times 5 \times 10^{-16} \; m^3$

$$=1.18 \; g_{/mL} \; \times 5 \times 10^{-10} \; mL$$

$$= 5.90 \; \times 10^{-10} \; g$$

As the mass ratio is 0.25 % for LDS750 in PMMA

Mass of LDS750 = $0.25\% \; \times (5.90 \; \times 10^{-10} \; g)$

$$= 147.5 \; \times 10^{-12} \; g$$

As we know the molar mass of LDS750 is 484 $g_{/mol}$, so mole

of calculated mass of LDS750 is = $\dfrac{147.5 \; \times 10^{-12} \; g}{484 \; g_{/mole}}$

$$= 0.305 \; \times \; 10^{-12} \; mole$$

So, the number of LDS molecule in $0.305 \; \times \; 10^{-12} \; mole$

$$= \; (0.305 \; \times \; 10^{-12} \; mole) \times (6.022 \times 10^{23})$$

$$= (1.84 \times \; 10^{12}) \; or \; (2 \times \; 10^{12})$$

Around one NDs matrix number of LDS750 dye is (2×10^{12}) approximate.
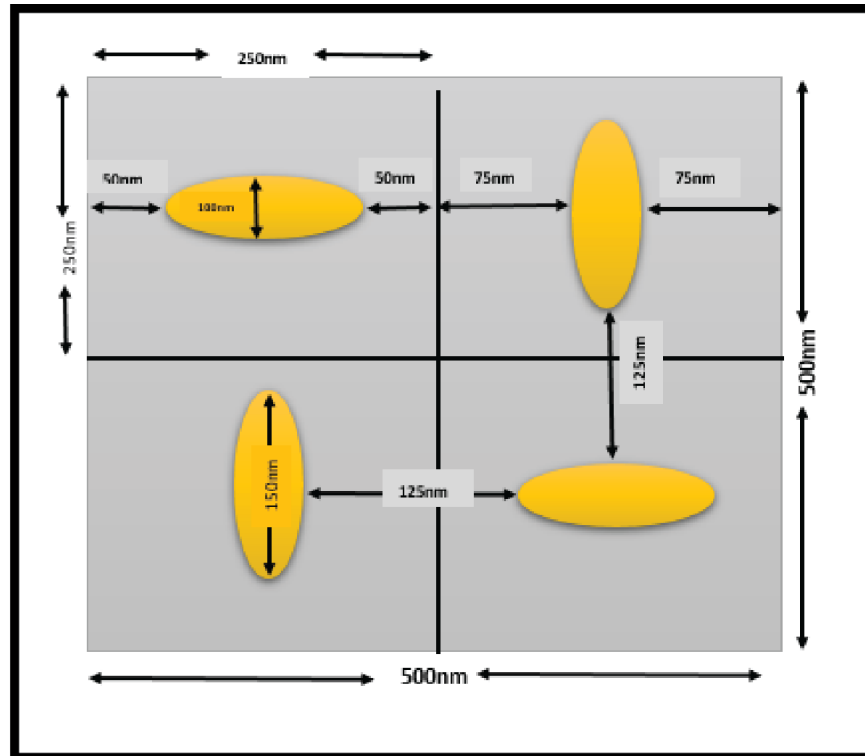
Figure 34. *Schematic of NEs design. Period of a unit cell is 500 nm with gap of 125 nm between NEs. The diameter of NEs is 100 nm and 150 nm.*